The
ENGINEERS' DIGEST

REVIEW OF ENGINEERING PROGRESS ABROAD

MAR 24 1945

VOL. VI. No. 2 FEBRUARY, 1945

EERING
RARY

In addition to all their other advantages, CHURCHILL Precision Roll Grinders are easily operated.

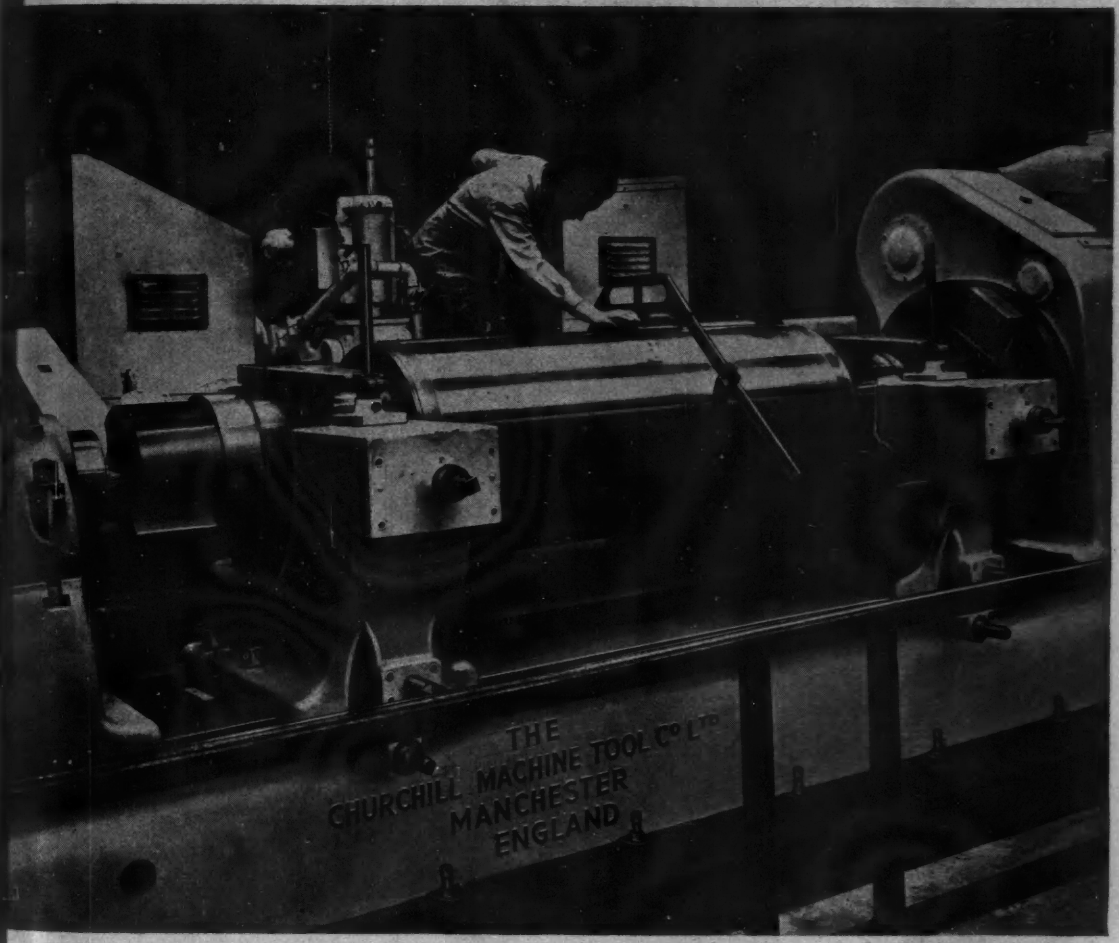

THE CHURCHILL MACHINE TOOL CO. LTD., BROADHEATH, Nr. MANCHESTER.

THE ENGINEERS' DIGEST

REVIEW OF ENGINEERING PROGRESS ABROAD

Published Monthly at 120, Wigmore Street, London, W. 1.

Publishers : **ENGINEERS' DIGEST LTD.** – – – – – – – Telephone : WELBECK 9357

Adverstisement Dept. – 120, Wigmore Street, London, W.1. – – Telephone : Welbeck 9357

Distribution – – E. & F. N. SPON, LTD., 57, Haymarket, London, S.W.1.
Telephone : Whitehall 1860. Telegrams : Fenspon, Lesquare, London

Editorial Dept. – – 120, Wigmore Street, London, W.1. – – Telephone : Welbeck 9357

Subscriptions to : ENGINEERS' DIGEST LTD., 120, Wigmore Street, London, W.1, or
E. & F. N. SPON, LTD., 57, Haymarket, London, S.W.1.

ANNUAL SUBSCRIPTION OF 12 NUMBERS, £2 2s. SINGLE COPIES, 4s. 6d.

ADVISORY COMMITTEE

J. F. ALCOCK, B.A., A.M.I.Mech.E.
R. W. ALLOTT, M.A., A.R.Ae.S.
E. ALTON, D.Eng., A.M.Inst.B.E.
H. H. ASBRIDGE, M.B.E., M.I.Mech.E.
R. W. AYERS, M.I.W.
Col. J. BOWDEN, M.Inst.C.E., M.I.Mech.E.
H. H. BROUGHTON, M.I.Mech.E.
F. BUCKINGHAM, B.Sc., A.M.Inst.C.E., A.M.I.Mech.E.,
T. H. BURNHAM, B.Sc. (Lond.), A.M.I.Mech.E. [A.M.I.E.E.
J. S. CASWELL, M.Sc., M.I.Mech.E.
G. C. SAFFERY COOPER.
J. DICK, Ph.D., B.Sc., A.M.I.Mech.E.
D. FIFE, M.I.Mech.E.
G. E. FOXWELL, D.Sc. (Lond.), F.Inst.P., F.Inst.F.,
R. GRIFFITHS, M.Sc. [M.Inst.Gas.E.
H. HEYWOOD, Ph.D., M.Sc. (Eng.), A.M.I.Mech.E.
O. HURST, M.Inst.N.A.
Capt. J. S. IRVING, M.I.Mech.E., M.I.A.E., A.F.R.Ae.S., M.S.A.E.
F. C. JOHANSEN, M.Sc. (Eng.), M.I.Mech.E., F.R.Ae.S., M.I.Loco.E.
W. J. KEARTON, D.Eng., M.I.Mech.E., A.M.Inst.N.A.
Prof. W. KERR, Ph.D., M.I.Mech.E.
G. V. LOMONOSOFF, Dr.Ing., M.I.Mech.E.
B. J. LYMER, M.I.Mech.E.
D. T. MacIVOR, M.I.Mech.E., M.Cons.E.
W. O. MANNING, F.R.Ae.S.
R. B. MATTHEWS, Wh.Ex., A.M.Inst.C.E., M.I.E.E., F.R.Ae.S.
Prof. A. L. MELLANBY, D.Sc., LL.D., M.I.Mech.E.
J. H. R. RATCLIFFE, B.Sc. (Eng., Hons.), M.I.Mech.E.
Col. C. W. D. ROWE.
W. A. SCOBLE, D.Sc., A.R.C.Sc., M.I.Mech.E.
P. W. SEEWER, D.E. (Zurich), M.Inst.C.E., M.I.Mech.E.
Prof. S. PARKER SMITH, D.Sc., M.I.E.E., A.M.Inst.C.E.
C. F. H. VERITY, A.M.Inst.C.E., A.M.I.E.E., A.M.I.Mech.E.
E. G. WALKER, F.C.G.I., B.Sc. (Eng.), M.Inst.C.E., M.I.Mech.E., M.Am.Soc.C.E.
Major F. L. WATSON, M.Inst.C.E., M.I.Mech.E.
G. WATSON, M.Inst.C.E., M.I.Mech.E.
C. H. WOODFIELD, M.I.Mech.E., M.I.Struct.E.
T. WRIGHT, Ph.D., M.Sc.
M. L. YATES, Ph.D., M.Sc.Tech., M.A. (Com.), M.I.Mech.E.

A "SABEN"
HIGH SPEED STEEL
10% SABEN TUNGSTEN
14% SABEN TUNGSTEN
18% SABEN EXTRA TUNGSTEN
22% SABEN KERAU TUNGSTEN
6% SABEN WUNDA COBALT
10% SABEN TENCO COBALT
FOR EVERY NEED
A low Tungsten Steel for Hot Die work. Special feature.—To withstand High Temperatures without cracking.
A good reliable High Speed Steel for Taps, Drills, Boring and Turning Tools, Punches, etc.
The Standard 18-4-1 High Speed Steel for all Metal Cutting Tools, Twist Drills, Milling Cutters, etc.
A Steel with just that extra bit of quality to tackle those special jobs that make hard going for lower Tungsten Brands.
For Machining Nickel Chrome Steels, High Manganese Steels and Castings.
For the toughest of all Machining Jobs. Specially recommended where customers' machines are not adapted for the use of Carbide Tools.
Our Booklet B.6 gives full details of these Steels, and is available on request.
THESE ARE ALL STANDARD QUALITIES TRIED TESTED AND PROVED WAR-TIME GOVERNMENT RESTRICTIONS MAY HAVE CAUSED THE TEMPORARY SUBSTITUTION OF OTHER ANALYSES, BUT SOME ARE STILL AVAILABLE, AND OUR SERVICES AND ADVICE ARE AT CUSTOMERS' DISPOSAL
SANDERSON BROTHERS & NEWBOULD LTD SHEFFIELD

Ana
Ani
Bral
The
Dete
Desi
Effic
The
The
Inves
Meas
Mech
A Ne

ACTARC

AR

FIRST
When the
correct a
plate, the
over the d
arc will
metal crat
Should th
too vertic
round it a
posited me
zontal, the
the plate,
deposit.

When de

With th
electrode is
movement
preceding b
bead alread
a flat pad.

For eas

CONTENTS

page

Analysis of the Combustion Process 44
"*The Engineers' Digest*," *Vol.* 6, *No.* 2, *p.* 44.

Aniline-Formaldehyde Resins and Laminates as Electrical Insulating Materials 34
"*The Engineers' Digest*," *Vol.* 6, *No.* 2, *p.* 34.

Braking Airscrew and High-Speed Flight 53
"*The Engineers' Digest*," *Vol.* 6, *No.* 2, *p.* 53.

The Combustion 39
"*The Engineers' Digest*," *Vol.* 6, *No.* 2, *p.* 39.

Detection of Flaws by X-Ray Fluoroscopy 29
"*The Engineers' Digest*," *Vol.* 6, *No.* 2, *p.* 29.

Design of Small Ceramic Components 31
"*The Engineers' Digest*," *Vol.* 6, *No.* 2, *p.* 31.

Efficiency of Compressed Air Plants by Use of Air Tools Operating on the Expansion Principle .. 35
"*The Engineers' Digest*," *Vol.* 6, *No.* 2, *p.* 35.

The Equilibrium Condition of Manometers of the Ring Balance Type 51
"*The Engineers' Digest*," *Vol.* 6, *No.* 2, *p.* 51.

The Influence on Tensile Strength of the Inclination of Weld-seams to the Direction of Loading 48
"*The Engineers' Digest*," *Vol.* 6, *No.* 2, *p.* 48.

Investigation of Mooring Rings 38
"*The Engineers' Digest*," *Vol.* 6, *No.* 2, *p.* 38.

Measuring Piston Bores of High Speed Internal Combustion Engines 33
"*The Engineers' Digest*," *Vol.* 6, *No.* 2, *p.* 33.

Mechanically Operated Auxiliary Switches for Contactor Circuits on Machine Tools 41
"*The Engineers' Digest*," *Vol.* 6, *No.* 2, *p.* 41.

A New Method for Measurement of very Small or Large Impedances at 300 to 30,000 MC/S .. 37
"*The Engineers' Digest*," *Vol.* 6, *No.* 2, *p.* 37.

ACTARC SUREARC

Hints on ARC WELDING **3**

REINFORCING (1)

FIRST make a straight run. When the electrode is held at the correct angle (70 deg.) to the plate, the slag will flow naturally over the deposited metal and the arc will be maintained in the metal crater and not in the slag. Should the electrode be held too vertical, the slag will flow round it and mix with the deposited metal. If held too horizontal, the arc will blow along the plate, causing an irregular deposit.

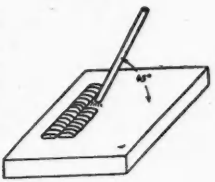

When deposit has cooled, remove all slag.

With the successive runs the angle of electrode is altered to 45 deg. The weaving movement is made from the top of the preceding head to about half the width of the head already made, so that the reinforcing is a flat pad.

For easy slag removal use Actarc Blue/Red and Red/White electrodes.

REINFORCING (2) **4**

FOR economy's sake it is often advisable to weld up or reinforce the worn parts on shafting by Arc welding.

The procedure is the same as for a flat pad, only the order of welding is as per diagram, always laying the preceding run diametrically opposite the bead just laid down.

Cutting tools can be built up after this fashion on Mild Steel shanks, using a hard surfacing electrode such as "Actarc" Violet/Green.

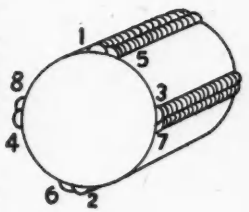

For good welding with minimum effort always use Actarc and Surearc electrodes. Approved by the main governing bodies.

ARC MANUFACTURING CO., LTD.

PROPRIETORS OF THE SUREARC ELECTRODE CO., LTD.

ACTARC WORKS, GOLDHAWK ROAD, LONDON, W.12.

Telephone : SHE 1151/3. Telegrams : Activarc, Phone, London

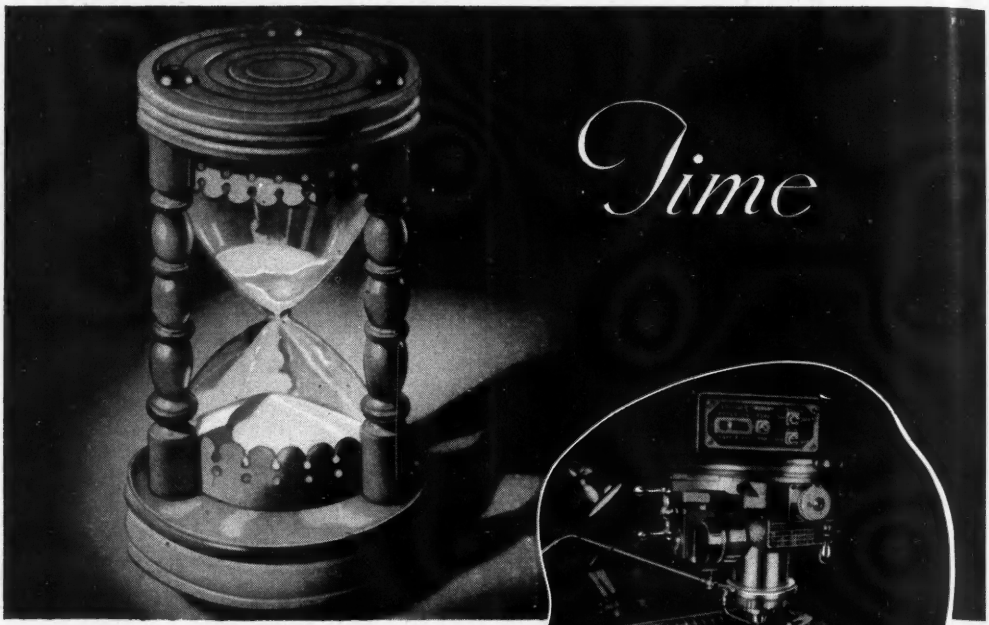

A "tricky" milling operation completed in far less time on THE KEARNEY AND TRECKER ROTARY HEAD MILLER

The most versatile machine ever designed for mould and die work, the Milwaukee Rotary Head Miller, equipped with a cherrying attachment, made "short work" of the "tricky" milling required on this injection mould. It took just two hours to complete the job—far less time than by any other method. The cherrying attachment is an auxiliary rotary head, mounted at 90° to the head of the machine. It is used to mill circles and angles in a vertical plane. When used with rotary head motion, spherical and conical cavities can be accurately and rapidly milled—in almost all cases difficult operations become a comparatively simple task.

Mould cavities can be machined in a single set-up without the aid of templates or models.

Chances of error are eliminated because there is no change in set-up. Exact control of all combinations of cutting movements—possible only with this machine—transmits mathematical precision to the work.

Initial job preparation and set-up time is reduced to the minimum. Accurate performance of the machine saves operator's time, and rapid production of intricate moulds and dies is ensured.

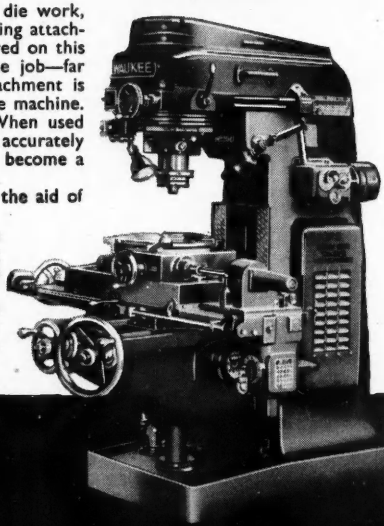

A.C. Wickman LIMITED

• COVENTRY • ENGLAND •

LONDON BRISTOL BIRMINGHAM MANCHESTER LEEDS GLASGOW NEWCASTLE

DETECTION OF FLAWS BY X-RAY FLUOROSCOPY.

By Dr. H. WITTE. (From *Zeitschrift des VDI*, Vol. 87, No. 33/34, August 21st, 1943, pp. 529-534).

IN the radiological examination of materials, recent years have witnessed an increasing employment of the fluoroscopic method in place of X-ray photography. Admittedly, the fluoroscopic method is a less sensitive means for the detection of flaws, but in many cases it is quite able to meet requirements. Moreover, for highly stressed parts the photographic method can be retained, while all other parts are examined fluoroscopically. This will result in a considerable saving of labour and film.

In connection with this tendency, the question arises as to what degree flaws can be detected by the fluoroscopic method. From the geometrical-optical aspect the problem can be considered as solved, since a relationship between the magnitude of the flaw, the size of the focal point of the X-ray tube and the magnification of the image, has been established. Less well-known, however, are the influences arising from the contrast, the brightness of the fluoroscopic screen and from the physiology of the eye.

A theoretical method to determine the smallest size of flaw, recognisable on the fluoroscopic screen, is as follows :

COMPUTATION BY CONTRAST AND SCREEN-BRIGHTNESS.

The X-ray tube may be assumed to emit a pencil of rays with a spectral intensity distribution of $\mathcal{J}_v = c\,(v_o - v)\,\Delta v$ (1), where $\mathcal{J}_v$ is the intensity between the frequencies v and Δv, and v_o is the frequency limit which can be found from the X-ray tube voltage U as $v_o = 2.43 \cdot 10^{14}\ U\ sec^{-1}$ (2) The constant C is determined by the material of the anode, the tube current and angle of incidence considered. The monochromatic radiation superposed over the continuous spectrum may be neglected, since its share in the total radiation is only small.

If the X-ray tube is operated by direct current, v_o will have a constant value, so that the intensity $\mathcal{J}_v$ is given by equation (1); but with other methods of operation, v_o will be a variable with time and the mean average intensity will then be expressed by $\mathcal{J}_v = \frac{c}{T}\int_{t_1}^{t_2} [v_o\,(t) - v]\,\Delta v\,dt$ (3) where T represents the time of duration of one cycle, and $(t_2 - t_1) \leq T$; while the integral may only be evaluated over such ranges in which $v_o\,(t) \geq v$. For the sake of simplicity, however, the case of direct current only will be considered here.

A pencil of X-rays possessing a spectral intensity distribution according to expression (1) may be assumed to be normally incident upon the work piece *a* which consists of a slab of thickness *d* as indicated in Fig. 1. This slab may contain a flaw of an extension *f* in the direction of the beam of rays. Beam *I* may by-pass the flaw, while beam *II* is shown as traversing it. The intensity of beam *I* within the spectral range between v and $v + \Delta v$ will then be reduced to $\mathcal{J}_{1v} = c\,(v_o - v)\,\Delta v e^{-\mu\,(v)\,d}$ (4), and that of beam *II* to $\mathcal{J}_{2v} = c\,(v_o - v)\,\Delta v e^{-\mu\,(v)\,[d-f]}$ (5), where $\mu\,(v)$ is the absorption coefficient of the spectral range extending from v to $v + \Delta v$.

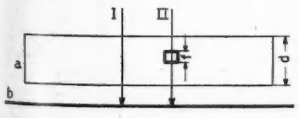

Fig. 1. **Passage of X-rays through investigated piece.**

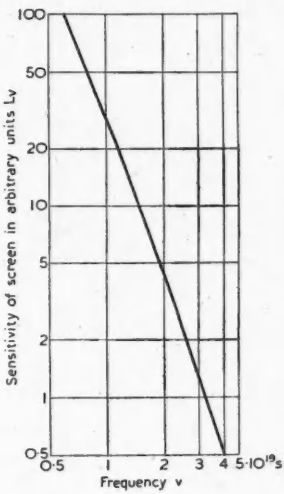

Fig. 2. **Screen sensitivity versus frequency of X-rays.**

The sensitivity of the fluoroscopic screen *b*, placed below the slab *a*, expressed by the brightness produced and based upon the unit of X-ray energy received, is a function of the frequency of the rays, the sensitivity rising sharply with increased frequency of the radiations received. This function is charted in Fig. 2. Taking L_v as the sensitivity of the screen for the spectral range from v to $v + \Delta v$, this range will contribute an amount $H_v = \mathcal{J}_v L_v$ to the total brightness of the screen; and this total brightness will be given by $H = \sum_v H_v = \sum_v \mathcal{J}_v L_v$

By the use of equations (4) and (5) the brightness of that part of the screen lying below the flaw is found as $H_F = \sum_v \mathcal{J}_{2v} L_v$ (6), and that of the ambient part of the screen as $H_U = \sum_v \mathcal{J}_{1v} L_v$ (7). The existing contrast is then given by $\frac{(H_F - H_U)}{H_U}$. If scattered radiation is also taken into account, the brightness of the screen will be $H + \alpha \cdot H$ and the contrast will, therefore, decrease to

$$k = \frac{(H_F + \alpha H_U) - (H_U + \alpha H_U)}{H_U + \alpha H_U} = \frac{H_F - H_U}{H_U + \alpha H_U} \quad (8)$$

This unfavourable decrease in contrast by scattered radiation is accompanied by an increase in brightness. But because of the contrast-threshold characteristics of the human eye, an increase in brightness permits the recognition of smaller contrasts, and the adverse effect of scattered radiation will, therefore, be largely cancelled out.

In order to save the considerable amount of work involved in a theoretical computation of α, the influence of scattered radiation was determined by a special test conducted with a 25 mm. thick aluminium slab of 6×9 cm. area. All theoretical computations made were based on this slab, which also served for the experimental investigations conducted into the recognizability of flaws. The values of α found for this slab were as follows :

100 kV : $\alpha = 0.42$	125 kV : $\alpha = 0.45$
150 kV : $\alpha = 0.48$	200 kV : $\alpha = 0.60$

These values were used to compute both contrast and relative screen brightness prevailing at 100, 125, 150, and 200 kV. The contrasts obtained for flaws with extensions of $f = 0.5$, 1.0 and 2.0 mm. in the direction of the X-ray beam were used for establishing the curves shown in Fig. 3, while the relative brightness values were found to be 1.89 at 125 kV, 2.91 at 150 kV, and 5.52 at 200 kV, based on a value of 1.0 at 100 kV.

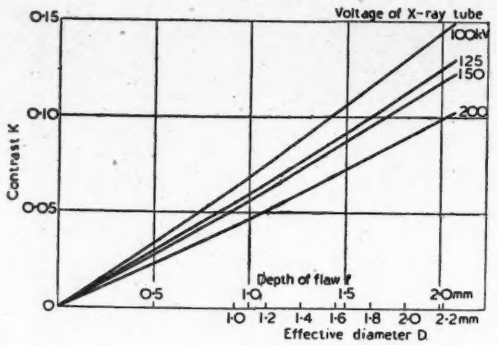

Fig. 3. **Contrast x/k versus depth f of flaw (continuous d.c.).**

THE PHYSIOLOGICAL FACTOR OF VISION.

In modern practice, the brightness of the screen lies below the range to which the Weber-Fechner law is applicable, and the magnitude of the smallest contrast detectable will, therefore, increase with the brightness of the screen. Also, with the small brightness values prevailing, the greater the brightness of the screen, the smaller the size of image of a flaw that can still be perceived by the eye. Whether a fault will be perceptible or not, can be determined from the contrast-threshold versus brightness relationship, which is charted in Fig. 4 for various sizes of flaws. Here the curves shown,

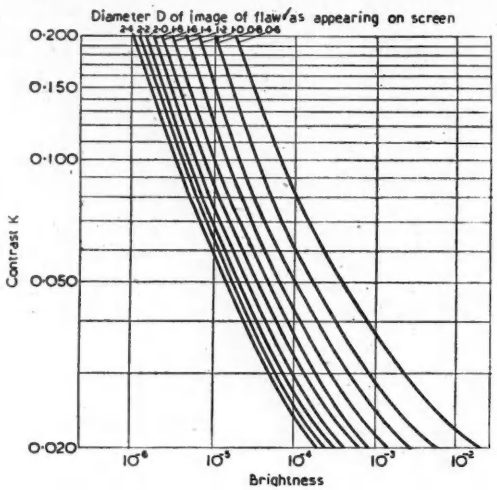

Fig. 4. **Visual contrast threshold values as function of brightness (according to H. Siedentopf).**

represent the minimum combination of brightness, contrast and image diameter, of the flaw that affords visual perception. Any other set of conditions, characterised by a point falling to the right of the corresponding curve, will denote visibility of the faulty spot, while all points to the left of the curve will indicate its invisibility.

COMPUTATION OF THE SMALLEST FLAW DETECTABLE BY VISUAL INSPECTION.

In the computation of the smallest flaw than can be detected on the screen by the human eye, it is necessary to differentiate between the real diameter of the flaw

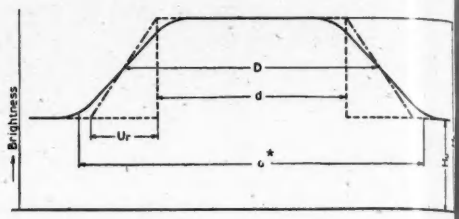

Fig. 5. **Definition of effective diameter D.**

(having the aforementioned depth f) and the apparent diameter D of its image on the screen. With regard to the brightness distribution on the screen (Fig. 5) it is clear that, if no blurred zone V_r peripheral to the image is present, the brightness of the image as shown on the screen would abruptly change at the periphery of the image from H_F to H_U (Fig. 5), the latter being the brightness of the free area of the screen. Qwing to both peripheral blur U_r and the inherent blur U_i of the screen, however, a gradual transition in brightness from H_F to H_U takes place, and the image diameter perceived by the eye will therefore be larger than d, although smaller than d^*. The effective diameter D may be arbitrarily assumed as that diameter for which, the difference $H_F - H_U$ is decreased by one-half. According to Fig. 5 it is $D = d_i U_r$. Furthermore, if the distance between the focal point of the X-ray tube and the flaw is taken as a, and the distance between flaw and screen as b, it will be

$$D = d + U_v = f\frac{a+b}{a} \quad (9).$$

In the numerical example on which Fig. 3 is based, the following values were chosen: $a = 91.5$ cm.; $b = 8.5$ cm. resulting in $(a + b)a = 1.093$. Referring to Fig. 3, it will be noted that in addition to the depth f of the flaw, the effective diameter D is also given.

The actual computation of minimum flaw visibility was made as follows:

As only relative brightness was considered, one single brightness value was determined from the experimental values of flaw visibility as given in Fig. 4. Thus, to a certain extent, the approach to the problem is based on the very result of its solution. However, as the chart Fig. 4 refers to white light only, the values found must be taken as equivalent brightness values, that is to say, as brightness values such as would be required to afford flaw visibility with a screen emitting white light. These equivalent brightness values can be found from the minimum flaw visibility value in question as follows: Taking for instance the test conducted at 100 kV and 30mA, the minimum flaw visibility value is given as $f = 1.45$ mm. where f represents the actual depth of the flaw still perceived by the eye. The effective diameter D of the flaw will, therefore, be $D = 1.093$; $f = 1.59$ mm. According to Fig. 3, this corresponds to a value of $K = 0.103$. With these values of K and D, an equivalent brightness of $7.95.10^{-6}$ Stilb. is found from Fig. 4. As the relative brightness values have been computed for different X-ray tube voltages, it is possible to establish an equivalent brightness value for each voltage and milli-amperage condition.

Once the equivalent brightness is known, the minimum size of flaw that can be detected can be ascertained from the chart Fig. 4. This is done by selecting the respective D curve, which, at the equivalent brightness value in question, calls for a contrast value equal to the contrast value actually existing indicated in Fig. 3 for the considered effective diameter D and voltage.

DESIGN OF SMALL CERAMIC COMPONENTS.

By J. WALLICH. (From *Zeitschrift des VDI*, Vol. 88, January 8th, 1944, pp. 9-14.)

A NUMBER of ceramic materials have been developed in recent years which satisfy the strictest requirements with regard to heat resistance, electric strength, low dielectric loss, and permanency of physical dimensions. The mechanical properties of these materials approximate to those of high-grade porcelain such as are used for electrical purposes. Components made of ceramic materials are used in mass produced apparatus and it is therefore essential that the designers of the apparatus involved should be familiar not only with the properties of the ceramic materials, but also with the aspects of their production. One of these aspects is the respective accuracy of dimensions that can be obtained with or without machining of the piece. The ceramic materials employed in high frequency technique are preponderantly of the magnesia-silica type which offers special advantages from the viewpoint of manufacturing technique. These materials can be moulded by any of the processes employed in ceramic practice, and they can be bonded in various ways with metallic conductors without requiring cements or glues. Furthermore, they can be fused to glass, making joints which are liquid, gas, and vacuum-tight.

The methods used in the shaping of ceramic components are fundamentally different from those applied to metals. Ceramic bodies are shaped from plastic or liquid masses in the cold state, their composition being closely controlled. The final properties of the material as well as the required dimensions are only attained after firing. After firing a ceramic component acquires its final immutable shape which cannot be altered by bending, since any excessive local stress would lead to deformationless fracture. Thus, for instance, when attaching unmachined surfaces of ceramic parts to supporting surfaces, the latter should be sufficiently elastic.

Another point to be kept in mind is the shrinkage which occurs in firing ceramic bodies. Even when due allowance is made in the dimensions of mould or template, variations in shrinkage cannot be avoided. In base plates or pieces, such as shown in Fig. 1, bolt holes should not be round, but elongated as indicated in Fig. 2.

The machining of fired pieces can be effected only by wet grinding with the use of high speed grinding wheels.

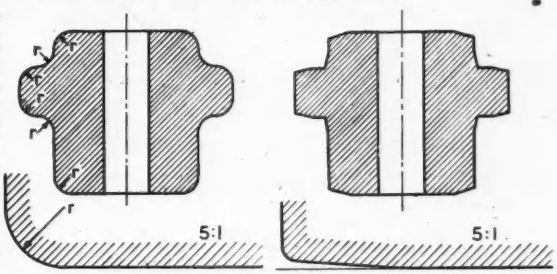

Fig. 3. **Wrong design of pressed part (at left hand side).** Large radii are undesirable.
Correct design of pressed part (at right hand side). Radii are kept small.

The technique of grinding to final dimensions is now so highly developed that with routine methods of grinding, accuracies of ± 0.01 mm. are attained. Even in mass production, grinding represents an entirely economic proposition. A parallelism of ± 0.03 mm. in 100 mm. can be obtained in the grinding of plane surfaces, while in the grinding of axles and shafts (centreless grinding being the usual method) deflection can be limited to 0.03 mm. over a length up to 700 mm., the limit rising to 0.04 mm. for pieces of greater length. Holes of 4 mm. diameter are the smallest that can be internally ground; the accuracy in this case amounts to ± 0.03 mm. Threads can also be produced by grinding, sharp thread profiles being preferable as it is difficult to shape wheels for the production of rounded-off threads.

The limits mentioned above represent average values, and if necessary can be reduced further in exceptional cases. Generally, the close tolerances given above will not be required and with components of simple shape and of normal size, the following limits of accuracy will suffice. These can be produced without machining the fired piece :—

± 3 per cent but not less than ± 0.3 mm. in production by casting or turning.

± 2 per cent but not less than ± 0.2 mm. to ± 0.3 mm. in production by wet pressing or by extruding.

± 1.5 per cent to 2.0 per cent but not less than ± 0.15 to ± 0.2 mm. in production by dry pressing.

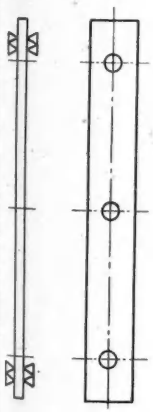

Fig. 1. **Wrong design.** Expensive to grind. Holes may not be at proper distance from each other because of shrinkage.

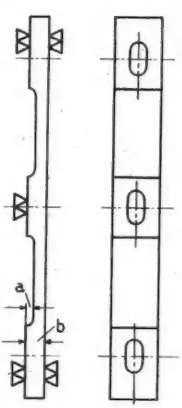

Fig. 2. **Correct design.** Less expensive to grind. Elongated holes obviate shrinkage difficulties.

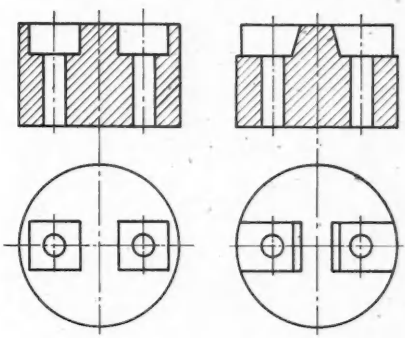

Fig. 4. **Wrong design of pressed part (at left hand side).** Wall thickness of square holes is too small. Wall will crack or break.
Correct design of pressed part (at right hand side). Outside walls of square holes omitted.

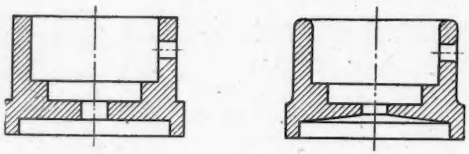

Fig. 5. **Wrong design of pressed part (at left hand side).** Sharp edges and high vertical walls yield a defective pressing. Horizontal bottom is subject to deformation.
Correct design of pressed part (at right hand side). Rounded off edges and slightly tapering walls ensure a perfect piece. The vaulted bottom does not suffer distortion.

It goes without saying that for economy's sake any surfaces to be ground should be kept as small as possible, but this point is not always sufficiently kept in mind. Clamping the piece for grinding can be considerably facilitated by providing small bosses for resting the piece in the correct position. Finally, it should also be noted that because of rapid wear of the grinding wheels, fillet radii of less than 0.6 mm. cannot be produced.

Wet or dry pressing in steel moulds is by far the most widely employed method of fabrication. Wet pressing consists in filling the mould with an excess of ceramic mass mixed with water and pressing-oil. This mass is compressed by the die to such an extent that the mould is completely filled, the excess being allowed to escape. In dry pressing the mould is filled with the exact quantity of dry ceramic mass required, no excess being permitted to escape. In dry pressing the mass is compressed to one-half its original volume. The dry pressed product has therefore a greater density and better electrical and mechanical properties than can be achieved by the wet pressing process. On the other hand, the dry material flows much less easily, and pieces with recesses and thin walls, etc., can only be made by the wet pressing method. But owing to the absence of shrinkage, dry pressed pieces are superior as regards uniformity and accuracy of dimensions. Also, the dry pressed pieces are more solid when lifted from the mould which makes dry pressing most suitable for automatic mass production. To achieve best results, care must be taken by the designer to adapt his designs to the exigencies of the pressing process. A few typical cases in which fabricating cost and quality of the product can be improved by simple changes in design are illustrated in Figs. 3-5.

In the extrusion process, tubes, rods, and all kinds of solid or hollow cylindrical bodies of considerable length are produced by pressing the plastic ceramic mass through a nozzle of the proper shape. Tubes up to 250 mm. diameter and 0.7 m. length, rods of 40 mm. diameter and 2 m. length, and rods of 75 mm. diameter and 1.5 m. length can be produced by this method. But small tubes of 4 to 12 mm. diameter with wall thicknesses as small as 0.2 mm., as used for high-frequency condensers in large quantities, are also made by the extrusion process. When designing a piece to be produced by extrusion, care must be taken to avoid sharp edges or corners, whilst a uniform wall thickness must be maintained in order to safeguard a uniform flow velocity throughout the nozzle area. A typical example of this is shown in Fig. 6.

The casting of complicated pieces, with or without core, can be carried out in plaster of Paris moulds which quickly absorb the water content of the slip poured into the mould. Considerations to be applied to the design

Fig. 6. **Wrong design of extruded piece (left hand).** Unequal wall thickness leads to warping.
Correct design of extruded piece (right hand).

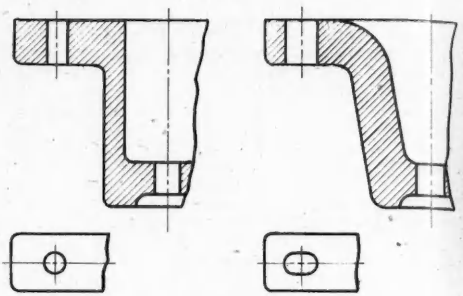

Fig. 7. **Wrong design of ceramic casting (left hand).** Unequal wall thickness leads to cracking of the piece, corner radii are too small. Round holes may not fit due to shrinkage.
Correct design of ceramic casting (right hand). Tapered shape, uniform wall thickness, elongated holes.

of ceramic castings are substantially identical with those pertaining to the casting of metals. The various points to be observed in the design of ceramic castings are exemplified in Fig. 7. Since the plaster of Paris moulds are worn out after 50 to 70 castings, this method of production is fairly expensive.

Large or highly complicated pieces are produced by making various component parts which are joined together with slip, so that they form one solid body after firing. This method must not be confused with that of joining fired biscuit parts by glaze. In this process, extensively employed in the manufacture of high frequency ceramics, the individual pieces of biscuit are prepared by grinding the surfaces to be joined, and the composite piece is then built up by means of templates. The assembly is then enamel-glazed in a muffle at 850-900 deg. C., which does not affect the component parts which were fired at 1400 deg. C. This building up of assemblies from individual pieces of biscuit joined together by enamel glaze, represents a great simplification of the manufacturing process and does away with the unavoidable inaccuracies by shrinkage experienced with parts made in a single piece. The increased cost of manufacture in making composite pieces will nearly always be cancelled out by the diminution of single piece kiln wasters and by the extraordinarily high accuracy of dimensions achieved. A

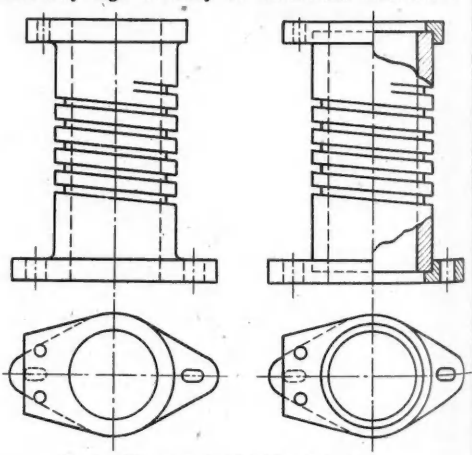

Fig. 8. **Wrong design (left hand side).** Single piece construction leads to kiln wasters because of distorted flanges.
Correct design (right hand side). Piece is built up from three separate grid pieces, assembled in jig and glazed together.

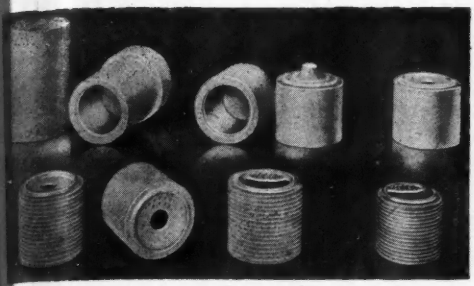

typical example of composite construction is illustrated in Fig. 8. The dimensions of pieces such as these are accurate within a few tenths of a millimetre as compared with the tolerance of ± 2 per cent required in single piece production. Even different ceramic materials can be joined in this way, provided they have identical co-efficients of thermal expansion. The connection of ceramic components to metal parts can be effected by the usual mechanical means ; and silver layers can also be applied direct to the ceramic surface by firing (Fig. 9). Where required, the thin layer of silver can be strengthened by electrolytic copper plating.

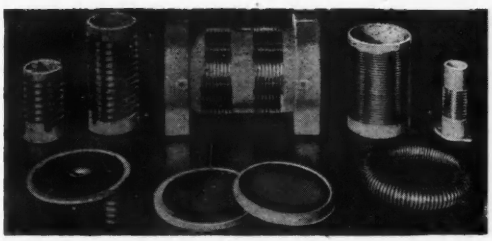

Fig. 9. Ceramic condenser plates and various types of coils with conductors fixed to the biscuit.

MEASURING PISTON BORES OF HIGH SPEED INTERNAL COMBUSTION ENGINES.

By Dipl.-Ing. A. MOSER, *VDI*, Stuttgart-Bad Cannstatt. (From *Werkstattstechnik*, *Der Betrieb*, Vols. 37/22, No. 5, May, 1943, pp. 197-198.)

SAFE working of the gudgeon pin in the piston bore has been attained by ensuring minimum tolerances of the order of 5-7μ between gudgeon pin and bore. This high accuracy can only be obtained in mass-production by further developing the methods of gauging.

USE OF PLUG GAUGES.

Until recently, standard gauges were considered satisfactory for measuring these bores for internal combustion engines. Plug gauges of the "Go and No go" type make it possible to reduce the total tolerance to 2-3μ, provided that skilled operators are employed. Results obtained from measurements with plug gauges depend to a large extent on the frictional changes occurring between the gauge and the bore, which might be caused by :—

(1) Surface roughness of the bore.
(2) Dirt in the bore.
(3) Type and thickness of film of used lubricant between the introduced gauge and the bore.
(4) Thickness of walls and material of the bore to be tested.

The inaccuracy of measurment due to these four factors may amount to as much as 5μ, which renders such gauges inadequate for present day jobs, because it is not only important to know whether the dimension is within the permitted tolerance, but also what are the exact sizes within the tolerance.

TESTING TOOLS OR EQUIPMENT.

Testing equipment of two kinds have been developed in the form of instruments with two and three point measurement, viz. :—

THE TWO POINT MEASUREMENT.

Nearly all measuring instruments of this type have one fixed and one adjustable measuring attachment (Fig. 1 left). Readings are obtained as comparative values to a calibrated gauge on an indicator dial. Hydraulic operated instruments, e.g., the Solex gauge, make it possible to compare measurements of the resistance of flow during discharge from two fixed nozzles.

THREE POINT MEASUREMENT.

In this method the piston rests on two fixed ledges, which form an angle of 120 deg. An adjustable feeler pin is located at the bisection of the angle (Fig. 1. right). The main advantage of this method of measuring is correct setting of the instrument in the bore, but results obtained with light metal bores differ when compared with two pin measurements, by several Microns. This is due to surface roughness and impurities which upset accurate measurements. To overcome this, the author fixed the feeler pin on the balance arm to both upper guide ledges opposite the two projections which are situated slightly higher than the ledges and the need or effect of the ledge attachment is dispensed with. The gauging of the bore takes place between three points ; the feeler point of the balance arm is interchangeable and permits the use of the instrument within a diameter range of about 5 mm.

Although the three point method of measurement is not absolutely necessary for inspecting piston bores, it is preferred because of simplicity of setting the instrument in the bore to be measured.

RESULTS ACCORDING TO AREA TOLERANCE LIMITS.

The diameters of the bores are sub-divided for fine measurement into several areas with tolerance limits of 2-3μ. Thus a higher degree of accuracy is obtained without having to resort to very fine tolerances during manufacture. A further advantage is that exact measurements can be read off directly as co-ordinated with one of the fixed area tolerance limits.

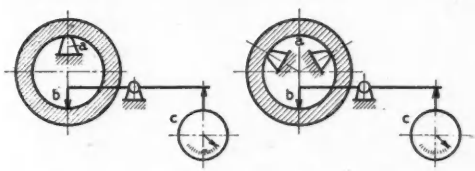

Fig. 1. Illustrates the method adopted for measuring piston bores by the two- and three-point system.

a = fixed measuring point.
b = moveable measuring point.
c = measuring instrument.

ANILINE-FORMALDEHYDE RESINS AND LAMINATES AS ELECTRICAL INSULATING MATERIALS.

By Dr.-Ing. LUDOVICO CODOLINI, Mailand. (From *Kunststoffe*, Vol. 33, No. 7, 1943, pp. 183-186.)

WHEN aniline is condensed with a larger proportion of formaldehyde in an acid solution, a resin is produced which can be used unfilled, filled or plasticised. The outstanding properties of these thermoplastic products are shown in Table I.

TABLE 1. PROPERTIES AND APPLICATIONS OF ANILINE MATERIALS.

Material	Most important properties (semi-finished)	Applications
Aniline resin unfilled	Homogenous, low losses at radio frequencies, not hygroscopic	Radio electrotherapy
Aniline resin + cellulose filler (50:50)	High insulating quality, low losses at telephone-frequencies, mechanical strength	Insulators for medium and high voltage
Aniline resin + asbestos filler (40:60)	Heat resistance, not hygroscopic	Shipbuilding
Aniline resin + plasticisers	Easy machinability, fabricating versatility, flexibility	Low voltage insulation

ANILINE RESINS FOR TRANSFORMERS.

For the application of electrical insulating materials in oil filled apparatus (oil insulated transformers, circuit breakers, etc.), the following requirements must be satisfied: resistance to hot oil, high dielectric strength, and low dielectric constant.

The practical advantages of using aniline resins when compared with standard phenolic materials for transformers are best illustrated by an example. Considering first the distribution of the voltage drop in the liquid and solid insulating materials in the transformer:

$$V_o = V \frac{S_o \cdot E_i}{S_o \cdot E_i + S_i \cdot E_o}$$

$$V_i = V \frac{S_i \cdot E_o}{S_o \cdot E_i + S_i \cdot E_o}$$

Hence: $$\frac{G_o}{G_i} = \frac{E_i}{E_o}$$

where: E_o = Dielectric constant of oil
E_i = Dielectric constant of the solid insulating material
S_o = Thickness of the oil film
S_i = Thickness of the solid insulating material
V_o = Voltage drop in oil
V_i = Voltage in solid insulating material
V = Total voltage
G_o = Specific pressure oil: V/mm
G_i = Specific pressure solid insulating material V/mm

When G_o is known, the pressure in the solid insulating material is also known.

With laminated aniline materials $Ga = \frac{2}{3} G_o$,

With laminated phenolin materials $G_f = \frac{2}{5} G_o$ and

the oil is exposed to a higher potential difference than with aniline material. It is obvious, therefore, that using laminated aniline of the same thickness as the phenolic material, the electric stress acting upon the oil is less, or, for the same insulating strength, less oil is required.

Example: In a 70 kV transformer, the phenolic tube insulation was 15 mm. and the oil film 35 mm. thick. Using laminated aniline the oil film thickness has been reduced to

$$35 - \frac{4}{15} \cdot 15 = 31 \text{ mm.}$$

without affecting the electric load on the oil film.

The electric pressure acting upon the tube has been increased from .68 kV/mm. (with phenolic material) to 1.04 kV/mm. As the dielectric strength of aniline

TABLE 2. MECHANICAL, THERMAL AND ELECTRICAL PROPERTIES OF ANILINE AND OTHER PLASTICS.

Material	Spec. weight g/cm3	Strength in bending kg./cm2	Impact strength cmkg./cm2	Hardness kg./cm2	Modulus of elasticity kg./cm2	Heat resistance Martens deg. C.	Distortion under heat deg. C.	Water absorption 7 days mg	Surface resistivity VDE 0302	Dielectric strength kV/mm.	Dielectric constant at 800 Cycl. 100 V	Dielect. loss tg $\delta 10^{-3}$ at 50 Cycl. 1500 V
Aniline resin unfilled	1.25	1,100	17—22	1400—1700	25,000	105—150	100—150*	25	20	30	3,5	5–7
Aniline paper laminations	1.35—1.4	1,500—1,800	25—30	1500	100,000	130—150	120—150	250	12	40–50	3–5	15–25
Phenolic resin wood filled	1.35	800	7	1300	80,000	130—170	130	250	8–11	8–10	5–7	40—300
Phenolic resin asbestos filled	1.8	600	6	1500	90,000 150,000	150—200	180	150	8–10	5	7	100—300
Phenolic paper laminated	1.35	1500—1800	25—30	1300	80,000—110,000	140—170	130	1500	9	20	5–6	50
Phenolic fabric laminated	1.35	1300—1500	40—50	1300	60,000—80,000	130—160	95	2000	9	6–15	5–6	50—600
Polyvinyl-chloride	1.4	1000	200—250	1000	30,000	60	—	30	12	25	3,5	15—18
Polystyrol	1.05	1000	18—23	1100	30,000	65	50	—	12	25	2–3	.2–.5
Cellulose-acetate	1.4	300—600	25—80	600	—	40—50	30	700—1000	12	20–30	3,5–7	20—70
Micanite	2.5	300	2–5	—	—	200	—	500—700	5	20	—	—

*150 deg. C. for recently developed new resin.

laminated material is twice as large as that of phenolic, there is no disadvantage attached to this change over.

Assuming that the transformer has an output of 500 kVA, with phenolic insulation the tube diameter would be 500 mm. and with aniline insulation only 492 mm., and all other dimensions will be correspondingly reduced. Moreover there is also a saving of oil up to 12 per cent.

If, for some reason, it is not convenient to alter the construction of the apparatus and reduce the oil content, a saving in insulating material can be effected by using lam nated aniline. In some cases the thickness of the insulating material has been reduced by 50 per cent.

Important applications of aniline materials are the surface properties especially when used in a humid or dusty atmosphere. Aniline resins are proved to have a sufficiently high resistance to surface currents.

Regarding inflammability, asbestos filled aniline material has practically the same quality as asbestos filled phenolic material.

SUBSTITUTE MATERIALS FOR MICA.

Owing to the war, there is a great shortage on mica in Europe. German and Italian technicians have, therefore, studied the problem of finding a substitute material for micanite materials and mica foils.

The micanite materials consist of mica and shellac. They have many applications in the electrical industry where high dielectric properties are required, and materials which can be considered substitutes for these products must have the following properties :

(a) high dielectric strength and resistivity
(b) high arc resistance and surface resistance
(c) low water absorption
(d) plasticity at elevated temperatures
(e) high heat resistance.

The outstanding properties of aniline materials are shown in Table 2 in comparison with other plastic materials. From this it is obvious that it can be used successfully. The economic advantages are also of importance : aniline is lighter and easier to machine than micanite.

The problem with mica foils is more difficult and in Italian practice mica foils are used mainly for collectors and for the wiring of stators and rotors in electric motors.

According to the Italian specification all insulating materials used for these purposes have to maintain their electrical insulating properties up to 120 deg. C.

Plastics with organic fillers are of no use, but experiments with aniline materials have proved very promising. Recently an aniline material has been developed with a heat resistance up to 200 deg. C. Leading Italian firms have built motors of medium and small size in which the collector sheets were insulated with this material with good results. The experiments are, however, not yet complete.

APPLICATION FOR CABLE INSULATORS.

Tri-acetate and glass fabric have been tried before. The former does not form a good bond with varnish. Glass fabric becomes brittle in the long run owing to vibration.

Aniline-resin products show more favorable results except that manufacturing costs are high, but there is every hope that this difficulty—being mainly a mechanical problem—will be solved.

EFFICIENCY OF COMPRESSED AIR PLANTS BY USE OF AIR TOOLS OPERATING ON THE EXPANSION PRINCIPLE

By A. BAUMANN. (From *Brown Boveri Review*, Vol. 30, No. 11, Nov./Dec., 1943, pp. 340-345).

THE overall efficiency of a steam turbine driven compressed air plant is made up as follows :

(a) Boiler	0.80
(b) Turbine (thermal)	0.25
(c) Compressor (isothermal)	0.65
(d) Piping (leakage)	0.90
(e) Consuming apparatus (adiabatic)	0.30—0.60

The overall efficiency is therefore equal to

$$0.80 \times 0.25 \times 0.65 \times 0.90 \times (0.30—0.60) =$$
$$0.035—0.070, \text{ that is } 3.5—7 \text{ per cent.}$$

This low overall efficiency cannot be greatly influenced by factors (a) to (d). Factor (e), the subject of this discussion, is liable to variation. The upper value of 60 per cent corresponds to the efficiency of compressed air reciprocating or rotating machines. The lower of 30 per cent to that of pneumatic hammers which—because of the need for low weight, simplicity, and avoidance of freezing—usually operate with little or no cut-off, i.e., expansion.

To expand air completely from the usual initial temperature and pressure of 30 deg. C. and 6 kg./sq. cm. abs. reduces the temperature of the exhaust air to about —100 deg. C., necessitating very thorough drying.

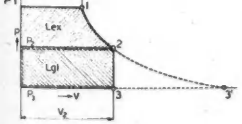

Fig. 1

The p–v diagram (Fig. 1) illustrates the effect of the cut-off on the air consumption and final temperature. 1 kg. of air at pressure p_1 is allowed to expand to pressure p_2. The left hand shaded area L_{ex} is the work associated with the drop in temperature during this expansion. The right-hand shaded area of constant volume L_{gl} between pressures p_2 and p_3., the back pressure (1.0 kg./sq. cm. abs.), has no part in this temperature drop, and the total work done by the air can be considered as the sum of the areas L_{ex} and L_{gl}. The heat content of L_{gl} manifests itself when the exhaust opens at the completion of the working stroke. The velocity energy then developed is shown by the area enclosed in the dotted lines, the portion 2—3—3′ being losses due to incomplete expansion. The temperature drop during the exhaust is regained and returned to point 2 at the end of the expansion and after dissipation of the velocity energy. This temperature drop at the end of the working stroke should not cause difficulties due to freezing, provided the exhaust openings have been suitably made.

The two work surfaces L_{ex} and L_{gl} may be expressed by means of the known expansion formulae for 1 kg. of air as follows, where

R = Gas constant
n = Adiabatic exponent
v = Specific volume in cu.m./kg.
T = Absolute temperature

(The indexes refer to the corresponding condition points of Fig. 1).

$$L_{ex} = p_1 \cdot v_1 \cdot \left[1 - \left(\frac{p_2}{p_1}\right)^{\frac{n-1}{n}}\right] \cdot \frac{n}{n-1}$$
$$= R.T_1 \cdot \left[1 - \left(\frac{p_2}{p_1}\right)^{\frac{n-1}{n}}\right] \cdot \frac{n}{n-1} \qquad (1)$$
$$L_{gl} = v_2 \cdot (p_2 - p_3)$$

TABLE I.

Pressure before expansion p_1 kg./cm.² abs.	6.0	6.0	6.0	6.0	6.0	6.0
Pressure after expansion p_2 kg./cm.² abs.	6.0	5.0	4.0	3.0	2.0	1.0
Adiabatic expansion work L_{ex} $(p_1—p_2)$ mkg./kg.	—	1530	3370	5500	8370	12400
Constant pressure work L_{gl} $(p_2—p_3)$ mkg./kg.	7400	6750	5920	4800	3210	0
Total work $L_{ex} + L_{gl}$ mkg./kg.	7400	8280	9290	10300	11580	12400
Heat value $A.L_{ex}$ kcal./kg.	0	3.6	7.9	12.9	19.6	291.
Heat value $A.L_{gl}$ kcal./kg.	17.3	15.8	13.8	11.2	7.5	—
Total $A.L_{ex} + A.L_{gl}$ kcal./kg.	17.3	19.4	21.7	24.1	27.1	29.1
Temperature t_2 after adiabatic expansion of dry air to p_2 deg. C.	30	15	—3	—24	—52	—91

with $$v_2 = \frac{R.T_2}{p_2} \quad \text{and} \quad T_2 = \frac{T_1}{\left(\frac{p_1}{p_2}\right)^{\frac{n-1}{n}}}$$

therefore

$$v_2 = \frac{R.T_1}{\left(\frac{p_1}{p_2}\right)^{\frac{n-1}{n}} . p_2} \quad \text{and} \quad L_{el} = \frac{R.T_1}{\left(\frac{p_1}{p_2}\right)^{\frac{n-1}{n}}} \left(1 - \frac{p_3}{p_2}\right) \quad (2)$$

$$L_{ex} + L_{gl} = R.T_1 \left[1 - \left(\frac{p_2}{p_1}\right)^{\frac{n-1}{n}}\right] . \frac{n}{n-1} + \frac{R.T_1}{\left(\frac{p_1}{p_2}\right)^{\frac{n-1}{n}}} . \left(1 - \frac{p_3}{p_2}\right) \ldots \quad (3)$$

Table I gives a summary of the values which interest us in this connection, basing on an initial pressure of $p_1 = 6$ kg./sq. cm. abs. and $t_1 = 30$ deg. C. as well as for expansion-pressures $p_2 = 6 — 1.0$ kg./sq. cm. abs. and with a constant back-pressure $p_3 = 1.0$ kg./sq. cm. abs.

Since the work figures are for 1 kg. of air, the extra air consumption due to incomplete expansion expressed in per cent of that with complete expansion, is given by the expression

$$\Delta G = \left[\frac{(L_{ex} + L_{g1})_{p_2}=1}{(L_{ex} + L_{g1})_{p_2}=x} - 1\right] . 100$$

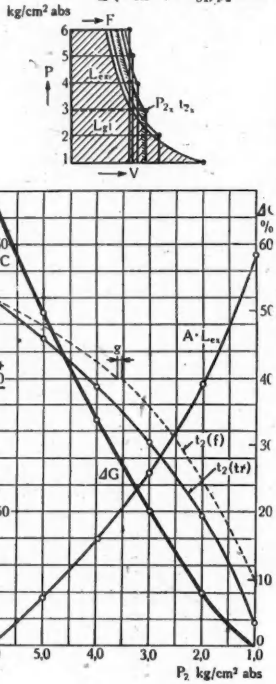

Fig. 2. **Additional air consumption, heat value of the expansion work, temperature at the end of the expansion with dry air t_2 (t_r) and with moist air to t_2 (f) with complete expansion from $p_1 = 6.0$ kg./cm.² abs. to 6.0—1.0 kg./cm.² abs. The curve ΔG shows clearly the way in which the air consumption increases with incomplete expansion as compared with complete expansion.**

A = Without expansion
B = Complete expansion
F = Position of cut-off.

Abscissae :

End pressure of expansion p_2.

Ordinates :

Heat value $A.L_{ex}$ of the expansion work L_{ex} in kcal./kg., t_2 (t_r) and t_2 (f) in deg. C. and the additional air consumption ΔG due to incomplete expansion to p_2 in per cent.

The heat values $A.L_{ex}$, taking part in the temperature fall during the working stroke, the final temperature t_2 (tr) for dry air and the extra air consumption Δ G are plotted in Fig. 2 as a function of the pressure p_2. Further, there is also included the curve t_2 (f) which corresponds to a definite moisture content and which is derived from the i–x diagram, referred to later (gain of the latent heat of condensation and of freezing of the deposited water). *It is seen therefore that with the full pressure diagram ($p_2 = 6.0$ kg./cm². abs) 67 per cent more air is required than with complete expansion.* The small p–v diagram, inserted at the top of Fig. 2, shows clearly the six different cases considered with the different points of cut-off, and it will be seen that the growing length of stroke with increasing expansion causes an increase in the weight of the tool.

The effect of the expansion on the formation of water and ice is represented on the Mollier i–x diagram (Fig. 3). The lines $\varphi = 1$ are drawn for the different pressures $p_2 = 1.0$–8.0 kg./sq. cm. abs. and indicate the dew points corresponding to different temperatures. Point 6 represents the initial conditions of the air before expansion at $p_1 = 6.0$ kg./sq. cm. abs. and 30 deg. C.,

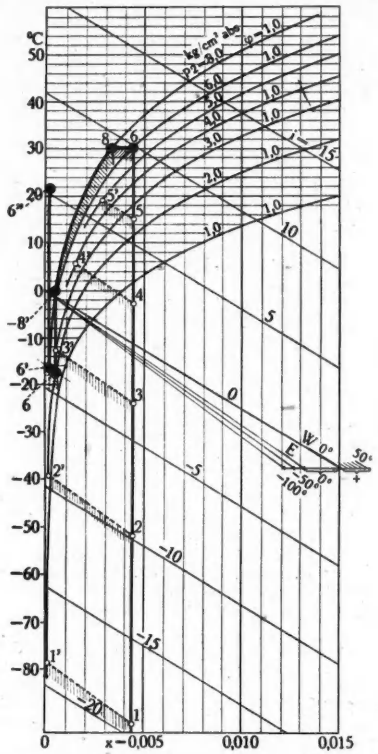

Fig. 3. **Representation of the expansion in the i–x diagram.**
Abscissae : Humidity x in kg./kg. dry air.
Ordinates : (oblique) heat content.
Border scale : W = Water E = Ice.

with 4.4 g. moisture/kg. air. If now we draw the values of $A.L_{ex}$, calculated under C., vertically downward, and draw from the end points (5, 4, 3, 2, 1) the fog- or ice-isothermals down to the dew line of the corresponding pressures p_2, then the points (5′ 4′ 3′ 2′ 1′) represent the state at the end of the expansion and in this way we obtain the real final temperature t_2 (f) at the end of expansion of moist air as indicated by the dotted line in Fig. 3. The hatching below the fog- or ice-isothermals denotes the separation of moisture which at temperatures below 0 deg. C. becomes ice. Under the stated conditions the temperature of 0 deg. C. is attained at an expansion pressure of $p_2 = 3.6$ kg./sq. cm. abs. According to Fig. 2 it will therefore be necessary to admit an additional air consumption of 28 per cent, *if it is desired not to go below the freezing limit. With a 67 per cent extra consumption (full-pressure diagram) there is no temperature drop and hence no deposition of water.*

Therefore it seems that a more efficient air drying would be worth while and the following methods may be used :

(a) Aftercooling and drying after the compressor with cold ground water.

(b) Drying with dehydrating agents, such as silicagel or carbagel, etc.

(c) Drying by means of refrigerating machines.

(d) Drying by " super-compression."

The cheapest of the above methods is that of (a). At 0 deg. C. the remaining humidity is only 0.5 g./kg., which would freeze only after expansion to very low pressure, but would not be likely to effect the tool. Cold water in the quantities required is not often likely to be available and the remaining methods, b, c, d, may be compared as shown in Table II.

Process *d* is illustrated on the *i–x* diagram (Fig. 3), by the broken lines (8–8′–6–6′–6″). The air, after being super-compressed to, say 8 kg./sq. cm. abs., is cooled to 30 deg. C. in an aftercooler and the condensate separated out. Compared to compressing the air to 6 kg./sq. cm. abs. this has an additional drying effect. A further drop in temperature to, for instance, 0 deg. C. is obtained by passing the air through a temperature exchanger effecting a further drying (8–8′), which leaves a moisture content of only about 0.5 g./kg. in vapour form. By expansion from 8 to 6 kg./sq. cm. abs. in an expansion turbine the temperature is reduced to —16 deg. C. and the moisture content almost eliminated, expansion taking place along the line (8′–6) and passing through the ice-isothermal (6–6′). The air is then returned through the temperature exchanger where it takes up the heat taken out on its first passage (Δi (8–8′) = Δi (6′–6″) with constant x) and its temperature is raised to 22 deg. C. (point 6″), thus eliminating all danger of freezing in the tool even with the most complete expansion.

TABLE II.

	b	*c*	*d*
Advantages	Practically unlimited drying without any direct power consumption	Low operating power	Simple operation using air only
Disadvantages	Periodic regeneration of the drying agent by heating, sensitivity of the material and possible renewal	More complicated operation with freezing medium and cooling circuit dilution of the brine solution and salt consumption	Larger power consumption

After deducting the expansion power recuperated, the extra power required for super-compression amounts only to about 10 per cent, compared to the maximum theoretical saving of compressed air which, according to Fig. 2, is 40 per cent of that required for full pressure pneumatic tools, when the air is completely expanded.

For compressed air plants the operating costs are about 10 per cent to 20 per cent of the capital charges ; a 10 per cent saving would therefore justify an increase in installation costs of 100 to 200 per cent. Air drying by super-compression and temperature exchanger should only involve an increase of 30 per cent in costs and would thus pay for itself in one to two years.

A NEW METHOD FOR MEASUREMENT OF VERY SMALL OR VERY LARGE IMPEDANCES AT 300 TO 30,000 MC/S.

By ALBERT WEISSFLOCH, Berlin. (From *Elektrotechnische Zeitschrift*, Vol. 64, No. 27/28, July, 1943, pp. 377-379).

THE methods of measurement of impedances in the region 300 to 30,000 Mc/s are based on the observation of the voltage distribution on a pair of parallel wires or a length of cable used as a " transmission line " (Fig. 1). The terminal impedance is then calculated from the situation of the wave minima, from the ratio $\frac{U_{max}}{U_{min}}$, and from the characteristic impedance of the " transmission line."

If the ohmic component of the impedance is large in respect to the other components, the ratio $\frac{U_{max}}{U_{min}}$ becomes so large that is is difficult to measure it directly. For such cases, another method is preferably used which consists in measuring the width of the nodes, which is defined as the distance between the points of the reading $\sqrt{2}\,U_{min}$ on either side of the minimum. From this distance the ratio $\frac{U_{max}}{U_{min}}$ and hence the terminal impedance (Fig. 1) can be calculated.

If, e.g., the terminal impedance is 1.5Ω, the wave length $\lambda = 15$ cm. (2000 Mc/s), and the characteristic impedance of the " transmission line " 75Ω, the width of the node as measured will be b = 1 mm. The same

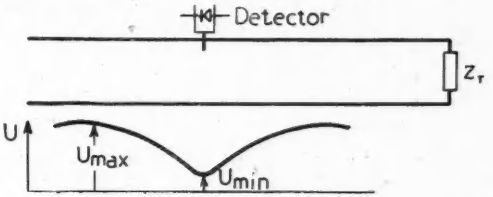

Fig. 1. **Determination of voltage distribution along a homogeneous conductor.**

width would, however, be measured if the load was $\frac{75^2}{1.5} = 3750\Omega$, and for loads under 1.5Ω or over 3750Ω the width of the node would be under 1 mm.

It is obvious that the accuracy of the measurement deteriorates rapidly when the width of the node decreases below 1 mm., the more so as the diameter of the detector contacts used for locating the nodes must be at least 0.5 mm. for purely mechanical reasons. Thus, limits are set to the application of this method, in particular when the terminal impedance is very small or very large compared with the characteristic impedance of the " line."

It may seem feasible to define the width of the node as the distance between the points, for instance, $\sqrt{5}\ U_{min}$ on either side of the minimum, instead of $\sqrt{2}\ U_{min}$ as mentioned before. This would certainly result in an increase of the distances to be measured and hence in an improvement of the accuracy. But there are certain limits in this case also.

Another way to increase the accuracy and to allow the smallest or largest impedances to be measured is by inserting a transformer between the load and the measuring wires, thereby transforming the impedance to a value where accurate measurement is possible. This method is shown schematically in Fig. 2.

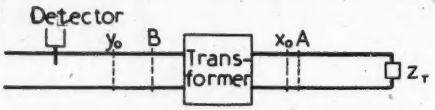

Fig. 2. Employment of transformation circuit for the determination of very small or very large impedances.

A homogeneous line, preferably of the same characteristic impedance as the measuring line, runs from the terminal impedance Z_T towards the measuring line. The value of Z_T is not constant along the line, but when measured progressing from Z_T towards the measuring line it appears as a vector turning in a clockwise direction. The locus of the tip of this vector will be a circle (Fig. 3). The point of intersection of this circle, with the real axis between the points 0 and Z represents the point with the voltage minimum, which on the real line, may correspond to point A (Fig. 2). At A, only the ohmic component of the terminal impedance Z_T appears, which there has the value $Z_{T\,min}$. If $Z_{T\,min}$ is very small compared with Z, ordinary methods of measuring the width of the nodes will be inaccurate or fail altogether, as described above.

Any four-terminal network connected to two pairs of homogenous lines of adequate length can be considered an "ideal transformer" if it is assumed that no losses will occur within the network. The "transformer" in Fig. 2 may be such that an impedance Z_2 connected at the point x_o appears as kZ_2 at the point y_o, the value of k being $k > 1$. It will be advantageous to have the "transformer" movable along the line. Thus, by shifting, the "transformer" x_o can be made to coincide with A and the terminal resistance $Z_{T\,min}$ will appear at y_o as $k.Z_{T\,min}$. If, e.g., $Z_{T\,min} = 0.5\Omega$ and $k = 20$, $k.Z_{T\,min}$ will be 10Ω. The width of the node at y_o will be approximately 20 times the corresponding value at x_o. The use of a "transformer" in this way enables terminal resistances of a much wider range than usual to be measured. It is irrevelant for the measurement, what kind of transformer is used, so long as no losses occur there, and if the ratio k as well as the points x_o and y_o are known. When measuring, special care must be taken to make x_o and A coincide exactly and to keep the frequency constant.

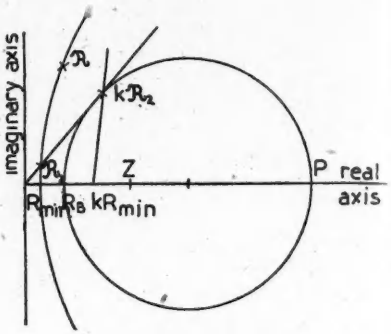

Fig. 3. Circuit diagram.

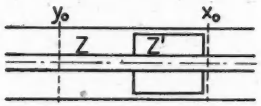

Fig. 4. Typical measuring circuit.

The simplest "transformer" is a homogeneous line $\lambda/4$ cm. long (λ = wavelength) whose characteristic impedance Z' is smaller than that of the measuring line. Then x_o is close to the right end and y_o about $\lambda/4$ in front of the left end of the "transformer." K will be approximately $k \approx \left(\frac{Z}{Z'}\right)^2$.

When measuring a line consisting of two concentric conductors the "transformer" can be obtained by pulling a cylinder $\lambda/4$ cm. long over the inner conductor (both must make good electric contact), and whose outer diameter is smaller than the inner diameter of the cylinder (Fig. 4). Thus, the homogeneous line with the characteristic impedance Z is "interrupted" by about $\lambda/4$ cm. length of line with the characteristic impedance Z_0 which serves as a "transformer" and which can be "moved along the line" simply by sliding the cylinder along the inner conductor.

No losses must be permitted to occur in the "transformer" and, therefore, to ensure electric contact of practically no resistance it is sometimes necessary to solder the cylinder to the inner conductor. In this case the position of the transformer cannot be adjusted accurately enough and it becomes necessary to bring about a sharp coincidence of x_o and A by slightly varying the frequency.

The article further describes the measurement of the ohmic resistance of a length of line consisting of concentric copper conductors, at $\lambda = 14$ cm., and refers to other publications for details.

INVESTIGATION OF MOORING RINGS.

By K. S. GNUDTZMANN. (From *Ingenioren*, No. 56, August 19, 1944, pp. B. 117-122).

IN order to determine the pull for which mooring rings should be tested, the Copenhagen Harbour Administration requested the State Testing Institute to test a number of rings made of different materials and of different ratio of ring thickness d to ring diameter D.

A number of typical test curves are reproduced in Figs. 1 and 2. Each of these curves is seen to exhibit a pronounced typical point at which deformation commences to increase considerably with the tensile load. From tests conducted on 14 rings of mild steel it was found that the pull at the "characteristic point" can be expressed by the relationship $T = k\frac{d^3}{D}$. In this equation, T is the pull in kg., d is the thickness of the ring in cm., and D is the mean ring diameter in cm., while k is a factor, the numerical value of which depends chiefly on the properties of the material and varies only slightly with the ratio $\frac{d}{D}$, as long as this ratio is kept within the

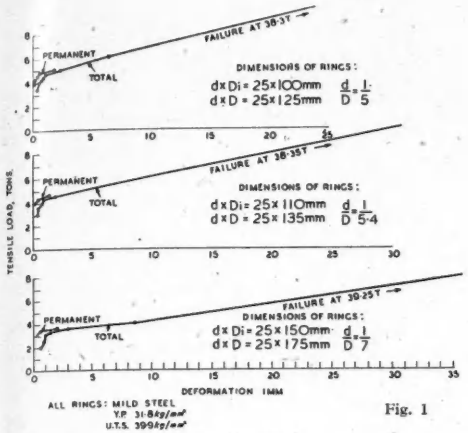

Fig. 1

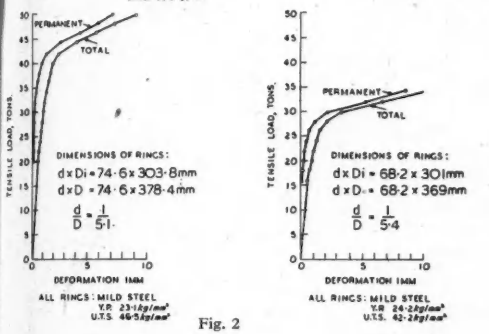

Fig. 2

limits of $\frac{1}{5}$ — $\frac{1}{7}$. For steel with a yield point of 31.8 kg. per sq. mm. and an ultimate tensile strength of 39.9 kg. per sq. mm., it was found k = 3,700, and for a steel with a yield point of 24.2 kg. per sq. mm. and an ultimate tensile strength of 42.2 kg. per sq. mm. it was found k = 3,400.

The permanent deformation which occurs at the "characteristic point" is insignificant and as a rule does not exceed 1.5 mm. in rings of the usual dimensions. The pull at the "characteristic point" has, therefore, been chosen as the test pull, the latter being determined as $T_t = 3{,}300 \frac{d^2}{D}$ for rings made of mild steel.

The maximum stress occurring with a pull of T kg. cannot be computed by the usual methods, since Hooke's law does not apply to a case of this kind. However, an approximate computation was made with regard to one of the rings tested, its thickness being 68 mm. and its

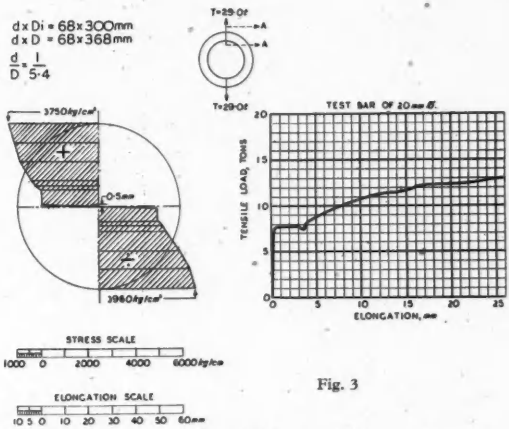

Fig. 3

interior diameter being 300 mm. The maximum moment caused by the pull T was taken as $M_{max} = T\frac{D}{2}$ where D is the mean diameter of the ring. On the basis of identical outer and inner moments, the stress distribution in this ring was established from the test data neglecting cross-sectional deformation. The stress distribution as found in this way is charted in Fig. 3, where the neutral axis is seen to have suffered a displacement of 0.5 mm. for a maximum tensile stress of 3,750 kg. per sq. cm. and a corresponding compression stress of 3,960 kg. per sq. cm.

In order to determine the fatigue strength of such rings, five mild steel rings of 25 mm. thickness and 100 mm. inner diameter were tested, their elastic limit being 25.6 kg. per sq. mm. and their ultimate tensile strength being 39.6 kg. per sq. mm. The pull at the "characteristic point" was determined as 4,150 kg. The fatigue tests were carried out at a frequency of 1,000 cycles per minute, the length of test being 2 million cycles. The results were as follows:

Max. pull Po, kg.	Min. pull Pu, kg.	Amplitude Pa = (Po—Pu)/2 kg.	Cycle to fracture
4,150	500	1,825	175,000
2,750	500	1,125	668,000
3,300	1,650	825	1,224,000
3,300	2,000	650	>2,000,000
3,300	2,200	550	>2,000,000

In all cases, fracture occurred at the welded joint. It will be seen that the rings are unsuitable for cyclic load variations of large amplitude. As shown by the table given above, with a max. pull of 3,300 kg. corresponding to 80 per cent of the pull recorded for the characteristic point, and an amplitude of 650 kg. the ring withstood 2 million cycles without failure. Applying this result to a ring of for instance 3", statically tested at 40 tons, it would appear that this ring can withstand fluctuating pulls varying between 19-32 tons. over a long period.

THE COMBUSTION SQUARE

By WA. OSTWALD, Heppenheim a.d. Bergstrasse. (From *Die Chemische Technik*, Vol. 16, No. 9, May, 1943, pp. 82-84).

IF carbon reacts in a producer with oxygen and water vapour at high temperature, CO_2, CO, and H_2 are formed in varying proportions, depending on the conditions under which the reaction takes place. These conditions are: temperature, time of contact, activity of coal, concentration, pressure, etc., while the nitrogen from the air passes through without undergoing any reaction. Reactions, such as the formation of CH are of no practical importance. If it is possible to gain exact knowledge and understanding about the reactions taking place between C_1 O_2 and H_2 O_D, then this will be very helpful in the use of tar-forming fuels.

The results of the reactions with carbon can be completely represented by the following four equations, irrespective of equilibrium conditions being reached and not taking into account the intermediate products formed, and the order in which the reactions take place:

$$\begin{aligned} &1.\ C + O_2 &&= CO_2 \\ &2.\ C + O_2/2 &&= CO \qquad .. \quad .. \quad (1) \\ &3.\ C + 2H_2O &&= CO_2 + 2H_2 \\ &4.\ C + H_2O &&= CO + H_2 \end{aligned}$$

Any gas composition, calorific value, thermal

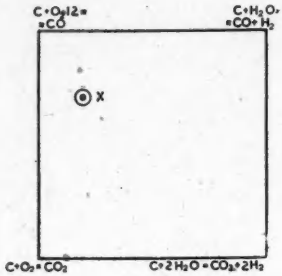

Fig. 1. **Locus of point "X" relative to the four corners is determined by the magnitude of the influence exerted by the four corner reactions.**

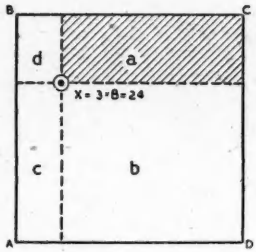

Fig. 2. **The extent of the influence exerted by reaction A is a measure of the surface area of the rectangle a.**

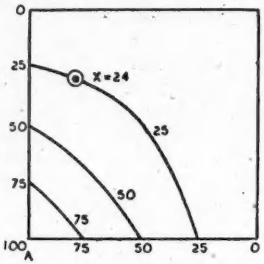

Fig. 3. **Hyperbolic net for assessing the influence of reaction A.**

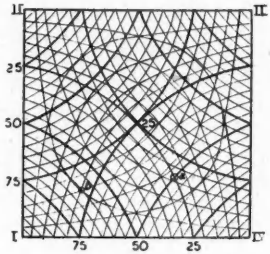

Fig. 4. **Hyperbolic net complete. Points (a) and (b) refer to examples**

I a = 25.0 per cent
b = 60.0 per cent
II a = 7.85 per cent
b = 15.0 per cent
III a = 16.7 per cent
b = 5.0 per cent
IV a = 50.0 per cent
b = 20.0 per cent

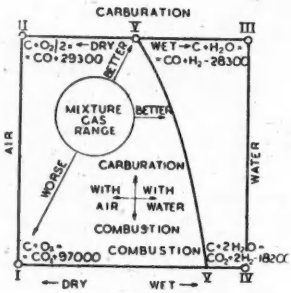

Fig. 5. **Diagrammatic representation of carburation process.**

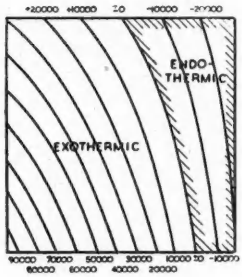

Fig. 6. **Exothermic vs endothermic reactions.**

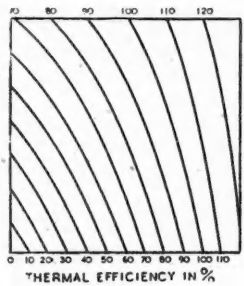

Fig. 7. **Determination of producer efficiency.**

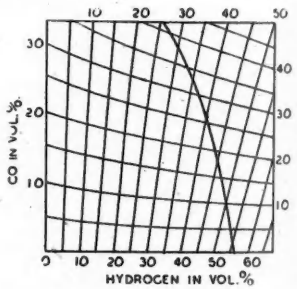

Fig. 8. **Representation of variation in gas analysis.**

No.	Reaction	Chemical Formula	Fuel: Incombustible CO_2	Fuel: Incombustible N_2	Fuel: Combustible CO	Fuel: Combustible H_2	Cal. Val. kcal/m³	Quantity m³/kg.C.	Cal. Val. kcal./kgC	Process Efficiency	Heat content kcal/kgC.
1	Combustion with air	$C+O_2(+4N_2)=CO_2(+4N_2)+97000$	20	80	—	—	0	9,33	0	0%	8080
2	Incomplete combustion with air	$C+O_2/2(+2N_2)=CO(+2N_2)+29300$	—	67	33	—	1 008	5,60	5640	70%	2440
3	Combustion with water	$C+2H_2O=CO_2+2H_2-18200$	33	—	—	67	1 720	5.60	9600	110%	—1520
4	Incomplete combustion with water	$C+H_2O=CO+H_2-28300$	—	—	50	50	2 795	3.89	10900	135%	—2360
5	Mixture combustion	$C+0{,}160_2+1{,}68H_2O(+0{,}63N_2)=CO_2+1{,}68H_2(+0{,}63N_2)\pm 0$	30	19	—	51	1 300	6.18	8080	100%	+ 0
6	Ideal mixture reaction	$C+O_2/4+H_2O(+N^2)=CO_2+H_2/2(+N_2)+500$	—	40	40	20	1 723	4.67	8040	99%	+ 42

efficiency of a generator, etc., can be represented by a definite relation of these four reactions, which are shown fully in the accompanying table. This could also be shown by the position of a point in a cube.

However, it is much plainer and simpler to use two dimensions only, similar to Gibb's triangle. This, naturally, would not be possible if, out of the four terms in the equation

$$a + b + c + d = 100 \quad .. \quad .. \quad (2)$$

three were always independent, in similar manner to Gibb's triangle where two are independent. In fact the four equations mentioned above (1) are by no means independent, there is a peculiar double-relation between them chemically and, therefore, mathematically also.

Equations 1 and 2 in (1) illustrate the reactions of carbon with oxygen, while equations 3 and 4 represent the reactions of carbon with steam. Equations 1 and 3 represent complete combustion of C (one with oxygen, the other with water), while equations 2 and 4 represent incomplete combustions of carbon, one with oxygen, the other with H_2O_n.

This peculiar double relation can be expressed mathematically by a second equation :

$$\begin{array}{ll} & a : b = d : c \\ \text{or} & a : d = b : c \quad .. \quad .. \quad .. \quad (3) \\ \text{or} & a : c = b : d \end{array}$$

As these two equations are valid, the relation between the producer equation can be illustrated plainly by what is called the " combustion square."

Each corner of the square in Fig. 1 represents one of the four reactions (going round the square in a clockwise direction). Obviously any point inside the square can represent the relation of four values which satisfies the two equations mentioned above. This relation is expressed numerically by the areas of the four rectangles formed by the co-ordinates of the point in the square. In Fig. 2 the position of the point X depends on A in such a way, that the area a of the rectangle diagonally opposite to the corner A, represents the amount (a = 3.8 = 24 hundredths) to which equation 1 (1) has contributed to the particular point of reaction.

It can easily be seen that the sum a+b+c+d+ is equal to the area of the square, and further that equation (3) is valid.

In the combustion square Fig. 3, the left hand bottom corner represents 100 per cent of reaction 1 (1), therefore, the remaining three corners have the zero value. If intermediate values are required, or if the equations of the co-ordinates are derived for equation 1 (1) a hyperbolic system of co-ordinates is obtained, shown in Figs. 3 and 4, which satisfies both main equations and permits the direct determination of the four numerical contributions by the four reactions for any particular point. There is no particular difficulty in taking a numerical reading ; in practice, however, this is not actually necessary. The meaning of the position of a point inside the square seems to be understandable without any numerical readings. For readings, charts of single or multiple functions of ordinary kind are used.

If these co-ordinates are used for the solution of combustion problems, a diagrammatic solution is arrived at as shown in Fig. 5. A " Neutrokalore " divides the square into an endothermic and an exothermic part. The ideal combustion (equation 6 in table) which as a rule is aimed at, is shown by the point VI on the combustion line. The points of the reactions taking place in actual practice are in the exothermic part. Obviously by means of this square, it is possible to see if combustion is taking place under favourable or unfavourable conditions ; what measures can be taken to improve conditions, and whether the improvement aimed at by the action taken would materialise and be sufficient.

Figs. 6, 7 and 8 illustrate a few examples of special charts. It is, of course, possible to make charts from which readings could be made, of gas per kg of carbon, calorific value of gas formed, CO_2 and N_2 content, and other properties of the gas.

MECHANICALLY OPERATED AUXILIARY SWITCHES FOR CONTACTOR CIRCUITS ON MACHINE TOOLS

By W. STAFFEL, Berlin. (From *Fertigungstechnik*, No. 2, May, 1943, pp. 25-29.)

Introduction.—Great progress has been made during past years in the development of electrical equipment for machine tools.[1] Multi-motor drives and specially designed control systems increase production and simplify the operation of the machines. Electrical control of the machine increases the working speed and all operations are made completely automatic, eliminating the human element as much as possible. There are machines already in service which have several elements working simultaneously and automatically, and few manipulations are required for commencing a new operation. This paper deals with the switches which play so important a part in maintaining a reliable service, and are subjected to very high stresses, both electrically and mechanically.

Application of the switches.—Stop switches applied to the electrical machine-tool drive prevent overtravel of reciprocating and rotating motions for purposes of safety ; they also serve for locking and, sometimes, also for setting the machine to work. The impulses are either of the continuous periodic type or are in synchronism with other motions. Such auxiliary switches are often employed in great numbers on the machine and may be fixed outside or inside, according to their function in co-operation with the mechanical elements.

Fig. 1 shows, diagrammatically, a plane miller. As will be seen the limit switches serve many purposes. On this machine, switch 8 protects the two vertical milling slides from colliding with each other. Switches 1 and 2 are provided for interlocking the hand-wheels ensuring the safety of the operator.

Fig. 2 illustrates the arrangement of a limit switch controlling a servomotor on a large machine tool. The movement of the actuating slide or ram is transmitted through a hand wheel which, when turned towards the " on " position, first puts-in the mechanical coupling and before the end position is reached, pushes home the slide of the switch. A similar device is frequently provided on medium size machine tools where hand operated throw-over gears or couplings require an interlocking or disengaging of the motors before changing-over. The actuating member is shown in Fig. 3. A boss is provided with two cams which meet the rams of the limit switches at the corresponding positions, thus making or breaking contact for the contactor control. Limit switches engaged in permanently supplying impulses are illustrated in Fig. 4. The rams are actuated through a cam shaft which, at a definite position of the working spindle, throws in auxiliary devices, such as boring slides, secondary drives, or additional boring or milling spindles.

On electrically controlled universal milling machines a number of limit switches control the direction of motion of the milling table and also its speed of motion (feed and quick-traverse). These switches will be discussed later.

The few examples described show that the requirements of the limit switches are manifold. Some work only 5 to 10 times per day, others have to carry out up to 2000 operations per hour. Not only the method of operation, but also the nature of assembling the switch with the machine varies greatly with the different types

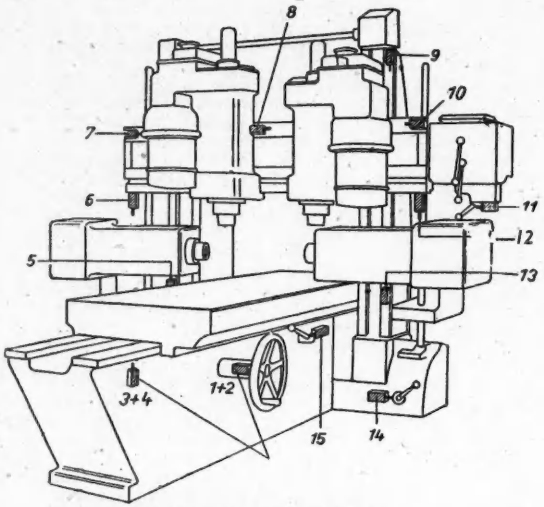

Fig. 1. Limit switches on a 4-spindle milling machine with table controlled mechanically.
1, 2: (On each side of the machine) switches interlock the hand-wheels which are coupled to the gear. Machine locked.
3, 4: (On each side of the machine) safety switches cut-out the table drive when mechanical stops are over-travelled.
5, 6 and 12, 13: "Limit of travel" end switches for left and right hand horizontal milling spindles.
7, 8 and 8, 10: "Limit of travel" end switches for left and right hand vertical milling spindles
6, 9, 12: "Limit of travel" for cross bar
11, 14, 15: Interlocking switches block the milling-spindle drive when the gear lever is in the "quick-travel" position.

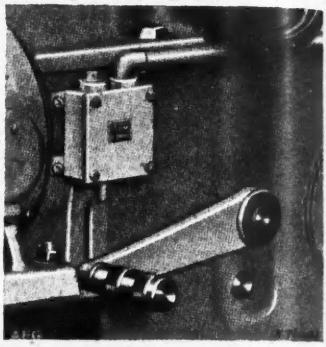

Fig. 2. Limit switch with cylindrical ram in sheet steel box. The switch blocks an electric drive when the coupling change-over crank is turned to the top position

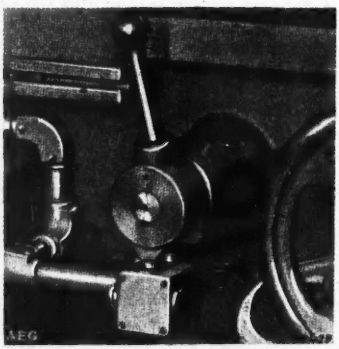

Fig. 3. Control lever for the table of a milling machine. The lever influences the mechanical and electrical controls. The two limit switches below the lever are cam actuated according to the lever position.

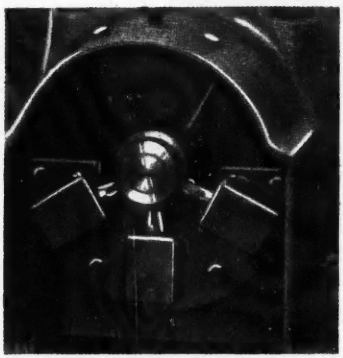

Fig. 4. Shaft end with cam disc which during rotation moves the rams of the 3 limit switches. The contacts are opened and closed in a definite sequence. The switches are protected by a specially shaped casing in the bearing pedestal.

of tools. The quality of the limit switch is determined by its contact system, the support of the ram and the nature of the protective enclosure.

Design of the limit switches.—In consideration of the many service conditions, the design of the switches, their mechanical strength and arrangement of the contacts cannot be standardized. The safety limit switches which are actuated occasionally, or in the event of failure of one section of the machine, can be kept essentially smaller in mechanical and electrical respect than continuously worked switches. Impulse contacts and actuating switches are naturally subjected to heavier wear on account of the greater number of operations. Switches are fixed on the machine in such a manner that they are reasonably protected against dust, water and oil, and fitted with a plain cover or casing, whilst, if this protection is missing, the switches must be mounted in a totally enclosed box. Open type limit switches may only be used when mounted inside the machine body.

As a rule, all limit switch constructions consist of an actuating ram, supported in two bores and carrying an insulating body with one or more contact bridges mounted thereon, which close the circuit over separate fixed contacts to which the connecting leads to the current source are clamped. By simple modifications or added contacts, a great number of combinations are possible, such as simultaneously closing or opening contacts in series. For inching motions, required for instance for slowly moving tables, quick-break limit switches are occasionally employed. Fig. 5 shows in elementary form, parts of the most commonly used types of limit switches.

Mechanically, the contact systems of the commercial patterns of end switches belong to one of three groups: (1) push contacts, (2) sliding contacts, and (3) quick-break contacts. In the first group, the two fixed contact points are closed by a rigid bridge, and the contact pressure, which reliably maintains the electrical contact, is produced by a laminated or, preferably a helical spring. In the case of the sliding contacts, the bridge moves clear of the fixed contacts during the closing or opening operations, at the same time cleaning the contact surfaces.

The quick-break type limit switches represent a special line. When the actuating ram begins its motion, the contacts remain stationary at first, whilst a spring is loaded which, when released, causes the bridge to move rapidly, thus resulting in an instantaneous closing or opening of the circuit.

Methods of assembling the switch with different classes of machine tools are manifold. Decisive, in the first place, is the nature of actuating the switch, i.e., its manner of co-operation with the corresponding machine element, and the mechanical construction of the ram. The assembly of the switch with the tool, and the combination with the moving members of the machine determine the amount of the stresses caused by lateral pressure on the switch which often may become so high that the plain pin shaped ram (Fig. 6a) cannot be

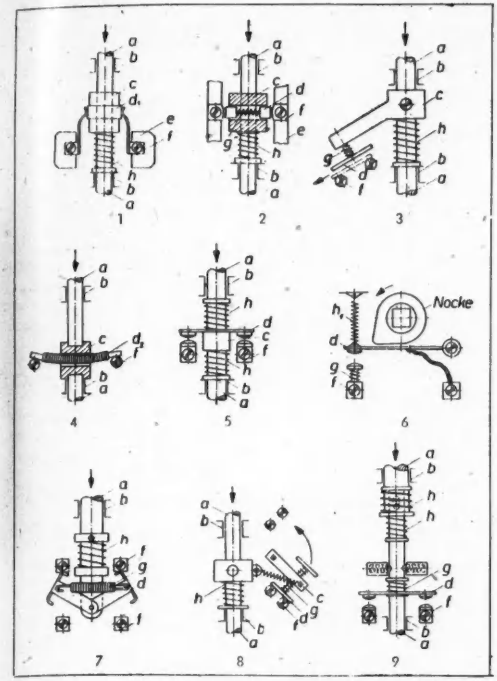

Fig. 5. **Construction of various commercial types of limit switches.**

1, 2, 3 : Limit switch with sliding contact
4, 5, 6 : Limit switch with press contact (ad 6 : cam)
7, 8, 9 : Limit switch with quick-break contact
(a) ram (b) ram guide (c) insulation carrier for bridge d (d) contact bridge (d1) contact ring (d2) worm contact (e) insulation base for fixed contacts (f) fixed contacts with terminal (g) contact push springs (h) return push spring (h1) return pull spring.

applied. When the impulse giving member of the machine, i.e., the cam, mounts the table from the side, the switches should be provided with rams carrying a roller or an angle lever roller (6 b, c, d). Lately, so-called cam limit switches with roller lever have been used (6e). The ram axle, connected to the lever, carries cam discs (Fig. 7) which, according to their shape, bring about the opening or closing of the circuits.

The contact systems.—Electrically, the limit switches can work on one of the three systems : (1) closed-circuit contact, (2) open-circuit contact, (3) change-over contact. In the "closed circuit contact" system the circuits are closed during operation. The circuits are opened during working in the case of the "open circuit contact" types. "Change-over contacts," with one or more poles, are made for opening and closing the circuits whereby their action may be overlapping, meaning that one or more contacts can be arranged for opening or closing at the same time.

The commercial types of limit switches are generally built for a voltage of 250, and must not be used for higher supply voltages which involves increased internal clearances and, consequently, larger overall sizes. The latest regulations for electrical machine tool equipment specify a control voltage of 220, thus setting up a standard for the electrical clearances and for the layout of the switch gear. Only air type switches are admissible for machine tool control. Contacts made of copper or brass are liable to become oxidised, particularly when working in a moist atmosphere. To prevent or minimise the formation of oxide, many designs provide wiping or sliding contacts for the switches, but in any case, a regular overhauling and removing the oxide skin will be necessary. Switches which, for some

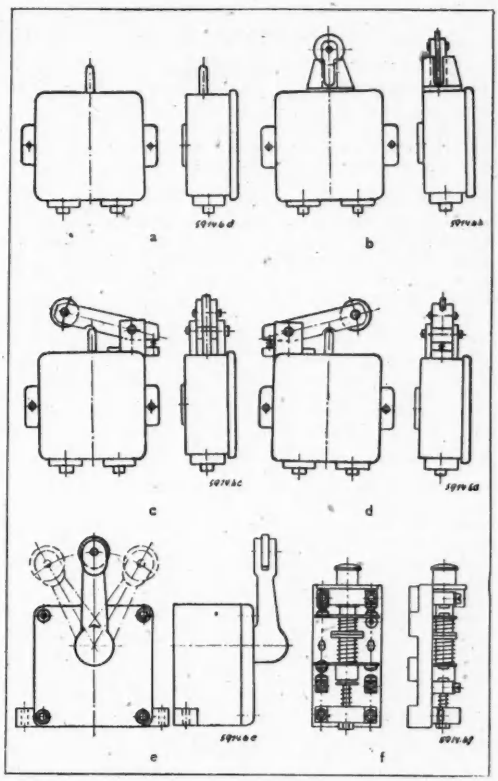

Fig. 6. **Various open and enclosed limit switch designs for machine tools.**

(a) switch in c.i. box with cylindrical actuating pin. (b) switch in c.i. box with ram carrying roller which can be turned by 90 deg. ; actuation from right or left hand side (control or curve disc must not be too steep). (c) switch as before with lever roller ; operation from right to left. (d) switch as c to be operated from left to right ; can be actuated from either side. (e) enclosed "cam switch" with roller lever used as table-travel and switch ; operation in either direction (f) open type limit switch ; operation by means of a roller lever which forms part of the machine tool.

reason, cannot be properly maintained will cause unsteady operation of the machine. Hence, the use of contacts made of precious metals, such as silver, is recommended, at least for switches controlling the more important sections of the tool.

REFERENCE.

(1) See W. Staffel : Standardized secondary controls for machine tools, *Werkst. u. Betrieb*," Bd. 75 (1942), No. 4, p. 84—New electric auxiliary switch for machine tools, *Elektrizitaetswirtschaft*, Bd. 40 (1941), No. 13, p. 227—Simplifying machine tool operation by centralizing the electric actuating switches, *Die Werkzeugmaschine*, Bd. 44 (1940), No. 17, p. 263.

Fig. 7. **Enclosed cam limit switch with roller lever ; smallest possible angle 20 deg.**

(a) For mounting outside on machine. (b) for fixing in recess inside machine; recess to be covered by front plate.

ANALYSIS OF THE COMBUSTION PROCESS

(From Professor T. M. Melkumov's Book, *Theory of the High-Speed Diesel*, Moscow, 1944, pp. 114-127.)

A theoretical investigation of the combustion process as it takes place in the cylinder of a diesel engine was carried out by K. Neumann, who has also devised a method of the kinetic analysis of the combustion process. According to the kinetic gas theory, chemical reaction can only take place by impacts of the molecules of the reacting media, which in the case considered are the fuel and the oxygen. Not every collision of molecules leads to reaction ; in order to destroy the chemical combination of the molecules with the original matter by a collision, it is necessary that there be set free a definite amount of energy which is termed the energy of activation and which is denoted by Qa. Therefore, of the great number of molecular collisions occurring only those will lead to reaction in which the collision energy is equal to or larger than Qa. The source of activation may be a central impact of two molecules, possessing at the given temperature the greatest velocity and, therefore, the greatest kinetic energy ; also, the source of activation may be a special molecular condition, in which the atoms, by virtue of a previous collision, possess a maximum of potential energy in consequence of the transition of the electrons to other orbits. The energy of activation also increases with rising temperature.
ture.

If Z_o is the total number of collisions taking place per second between the gas molecules contained per cu. cm. of mixture, then according to Boltzmann the number of collisions Z, which supplies the energy Qa of activation at the temperature T, is given by the expression

$$z = z_o \, e^{-\frac{Qa}{ART}} \quad .. \quad .. \quad (1)$$

where AR = 1.985 is the universal gas constant expressed in kal./kg. mol. deg. C.

The total number of collisions of two different molecules per cu. cm. per second is given by

$$z_o = 1.82 \cdot 10^{46} \cdot \delta_1 \, \delta_2 \, C_1 \, C_2 \sqrt{T \frac{\mu_1 + \mu_2}{\mu_1 \, \mu_2}} \quad .. \quad (2)$$

where δ_1 and δ_2 are the respective molecule diameters in cm., C_1 and C_2 are the concentrations of the reacting media, and μ_1 and μ_2 are their respective molecular weights.

Making $\delta_1 \, \delta_2 = \delta^2$ where δ is the mean geometric diameter of the molecules, and using a numerical value of $\delta = 3 \cdot 10^{-8}$ cm., and defining the number of collisions on the basis of kg-mol per cu. m. per second, it is

$$z_o = \frac{1.82 \cdot 10^{46} \cdot 10^6}{6.028 \cdot 10^{23} \cdot 10^3} \delta^2 \, C_1 \, C_2 \sqrt{T \frac{\mu_1 + \mu_2}{\mu_1 \, \mu_2}} \approx$$

$$\approx 2.7 \cdot 10^{10} \, C_1 \, C_2 \sqrt{T \frac{\mu_1 + \mu_2}{\mu_1 \, \mu_2}} \quad .. \quad .. \quad (3)$$

where $6.028 \cdot 10^{23} \cdot 10^3 = N_o$ is Avogadro number, that is to say, the number of molecules contained in 1 kg. mol of substance.

According to the law of active mass, the number of effective collisions between the molecules, or the speed of chemical reaction, is given by

$$z = k \, C_1 \, C_2 \quad .. \quad .. \quad (4)$$

where k is the constant of the speed of chemical reaction. By combining equations (1) (4) and (3) the expression for the constant of the speed of chemical reaction for the case of a bi-molecular reaction can be written thus,

$$= \frac{z_o \, e^{-\frac{Qa}{ART}}}{C_1 \, C_2} = 2.7 \cdot 10^{10} \sqrt{T \frac{\mu_1 + \mu_2}{\mu_1 \, \mu_2}} \cdot e^{-\frac{Qa}{ART}} \quad (5)$$

This expression is valid only for homogeneous reactions of the second order, that is to say, for the reaction of two molecular substances present in the gaseous or vapour phase. If in the wider sense it is assumed that in the mid-phase and the final phase of the combustion process, the reaction is homogeneous, that is to say, proceeds solely in the gas-vapour phase, then in the initial period the reaction is certainly heterogeneous, since the reacting substances exist in two phases, namely the gaseous and the liquid one. It will, however, be better to treat the combustion process of the diesel engine as one of the heterogeneous variety in all phases of combustion, and in the case of smoke production, even as one of the three-phase variety. However, these suppositions greatly increase the complexity of the kinetic analysis of the combustion process, as the knowledge of the kinetics of heterogeneous reactions is still insufficient.

In heterogeneous systems the gas molecules are adsorbed at the surface of liquid or solid bodies ; as the result of adsorption a partial chemical reaction may arise. However, the reacting molecules must be activated, that is to say, they must be imparted the required activating energy Qa. From tests it is known that the reaction in a heterogeneous system takes place quickly on occasion, even in such cases in which the adsorption of the gas at the surface of the liquid is very small. This permits the application of the theory of activation to heterogeneous systems also. Experiments have confirmed that the Arrhenius equation

$$\frac{d \log_e k}{d T} = \frac{Qa}{ART^2} \quad (6) \text{ or } \frac{d \log_e k}{d T} = \frac{Qa}{4.574 \cdot T^2} \quad (7)$$

does not only apply to homogeneous systems, but is also applicable to heterogeneous systems. In the latter case k represents the apparent constant of the speed of the chemical reaction. As in our computations the adsorption of molecules is not taken into account, the value for Qa will deviate from that for the true energy of activation.

The apparent constant of the speed of heterogeneous reaction can be obtained in the following manner. It can be assumed that all those gas molecules are subjected to chemical transformation which by collision with surfaces of the substance existing in the other phase have acquired the necessary energy of activation. If Z_o is the total number of collisions, the number of effective collisions per sq. cm. of surface per sec. leading to reaction will be the same as that found for the case of homogeneous reaction, that is :

$$z = z_o \, e^{-\frac{Qa}{ART}} \quad .. \quad .. \quad (1)$$

The total number of collisions can be expressed by

$$z = k_o C, \quad .. \quad .. \quad .. \quad (8)$$

where k_o is the constant of the speed of reaction for the total number of collisions of the gas molecules with the surfaces of the other substance existing in another phase ; while C is the gas concentration. The actual velocity constant of reaction is given by

$$k = k_o \, e^{-\frac{Qa}{ART}} \quad .. \quad .. \quad (9)$$

If n is the number of g-mol of gas in the volume V (cu. cm.), the concentration is given by

$$C = \frac{n}{V} = \frac{p}{RT} \text{ g-mol/cu. cm.} \quad .. \quad .. \quad (10)$$

where p is the pressure in g/sq. cm., T is the temperature in deg. Kelvin, and R amounts to 84,800 g cm/g-mol, deg. C., representing the universal gas constant.

The total number of molecules contained in

one cu.cm. of gas is given by

$$m = CN_o = N_o \frac{p}{RT}$$

where N_o is the Avogadro number, the numerical value of which is $6.028 \cdot 10^{23}$ molecules per gram mol of gas.

The number of collisions taking place per sq. cm. per surface per second, based on the number of gas molecules per cu. cm. of volume is given by $z_o = \frac{m \cdot v}{6}$, where v is the root mean square velocity of the gas molecules.

According to the kinetic gas theory, it is $v = \sqrt{\frac{3 R_k T}{\mu}}$, where $R_k = 8.313.10^7$ eng. per g-mol, deg. C, and μ is the molecular weight of the gas. Therefore, $Z_o = \frac{\sqrt{3}}{6} . N_o \frac{P}{R} \sqrt{\frac{R_k}{T\mu}}$

By expressing the number of collisions not by the number of molecules, but in terms of g-mol, and introducing the velocity distribution according to Maxwell, we obtain, $z_o' = \frac{1}{\sqrt{2\pi}} . \frac{p}{R} \sqrt{\frac{R_k}{T\mu}}$, the factor $\frac{\sqrt{3}}{6}$ being replaced by $\frac{1}{\sqrt{2\pi}}$.

From equation (8) and (10) it follows that

$$k_o' = \frac{z_o'}{C} = \frac{1}{\sqrt{2\mu}} \sqrt{R_k . \frac{T}{\mu}}$$

On the basis of 1 sq.m of surface of the reacting substance being in the liquid or solid phase, and on the basis of 1 cu.m. of gas, we have

$$k_o'' = \frac{10^4 . 10^6}{\sqrt{2\pi}} \sqrt{R_k \frac{T}{\mu}}$$

According to the computations carried out by Inozemtsev,

$$k_o'' = 3.72 \cdot 10^{-2} \sqrt{\frac{T}{\mu}} \quad .. \quad .. \quad (11)$$

and therefore,

$$k'' = 3.72 \cdot 10^{-2} \sqrt{\frac{T}{\mu}} . e^{-\frac{Qa}{ART}} \quad .. \quad .. \quad (11a)$$

The constant of the speed of a heterogeneous reaction in the cylinder of a diesel engine, based upon 1 cu.m. of gas and an area f of the surface of all fuel droplets encountered in 1 cu.m. of gas, is given by $k' = k'' f$, where $f = F/V$. Here F represents the total surface of the droplets present in the cylinder, and V is the cylinder volume. Assuming the droplets to be of spherical shape, it can be written $F = \frac{3B}{\gamma_T r_T}$, where B is the quantity of fuel in liquid state contained in the cylinder at a given instant, γ_T is the specific gravity of the fuel expressed in kg. per cu. m., and r_T is the average radius of the droplets in m. If r is given in cm. and γ_T in 0.1 cu. m., we find $F = \frac{3B}{10 . \gamma_T . r_T}$.

For 1 cu. m. of gas, $f = \frac{F}{V} = \frac{3B}{10 . \gamma_T . r_T . V}$

and therefore,

$$k' = \frac{3B}{10 . \gamma_T . r_T . V} . 3.72 . 10^{-2} \sqrt{\frac{T}{\mu}} . e^{-\frac{Qa}{ART}}$$

$$= 1.115 . 10^{-2} . \frac{B}{\gamma_T r_T V} \sqrt{\frac{T}{\mu}} . e^{-\frac{Qa}{ART}} \quad (12)$$

But as $\frac{B}{\mu_T V} = C_B$ kg.-mol/cu. m. where μ_T is the molecular weight of the fuel, and C_B is the concentration of fuel at the instant considered,

$$k' = 1.115 . 10^{-2} \frac{\mu_T}{\gamma_T r_T} C_B \sqrt{\frac{T}{\mu}} . e^{-\frac{Qa}{ART}} \quad .. \quad (12a)$$

The final products of reaction, that is, the carbon dioxide and the water vapour, are not formed all at once. But this computation does not touch upon the intermediate stages of the chemical transformation and only encompasses the range of equilibrium conditions. On the basis of the supposition that the chemical combination is the result of the collision between the molecules of fuel and oxygen, the reaction speed can be established as

$$z = -\frac{d C_B}{d \tau} = k . C_B . C_{o_2} \quad .. \quad (13)$$

where C_B and C_{o_2} kg. mol per cu. m. are the respective concentrations of fuel and oxygen in the cylinder, and $-\frac{dC_B}{dt}$ kg. mol per cu. m. sec. is the diminution of the fuel concentration after unit time; $k = k_o e^{-\frac{Qa}{ART}}$ is the constant of the actual speed of the chemical reaction according to the number of collisions, and k_o is the constant of the speed based on the number of collisions according to the kinetic gas theory.

For homogeneous gases the actual constant of reaction speed, k, is determined by equation (5). For a heterogeneous system $kC_B = k'$ where k' is obtained from equation (12a). For heterogeneous systems it is, therefore, necessary to introduce the apparent constant of reaction speed,

$$k = \frac{k'}{C_B} = 1.115 . 10^{-2} . \frac{\mu_T}{\gamma_T r_T} \sqrt{\frac{T}{\mu}} e^{-\frac{Qa}{ART}} \quad .. \quad (12b)$$

The introduction of fuel into the cylinder may be expressed by the equation $\sigma = f(\varphi)$ where σ is the total amount of fuel introduced while the crankshaft passes through an angle $\varphi°$. The rate consumption of fuel by the combustion process may follow the law $x = f_1(\varphi)$.

If B_o is the total amount of fuel in kg. introduced into the cylinder during one cycle, V is the cubical contents of the cylinder in cu.m. at a given instant, and if μ_T is the molecular weight of the fuel, the concentration of the fuel will then be given by,

$$C_B = \frac{(\sigma - x) B_o}{\mu_T V} \text{ kg.-mol per cu. m.} \quad .. \quad (14)$$

The concentration of the oxygen is determined as

$$C_{o_2} = \frac{0.21 . L . B_o}{V} - \frac{0.21 . x . L_o B_o}{V} \text{ or}$$

$$C_{o_2} = \left(\frac{1}{\beta} - x\right) \frac{0.21 L_o B_o}{V} \quad (15)$$

where β is the degree of utilisation of the air and L_o is the quantity of air in kg.-mol theoretically required for the combustion of one kg. of the fuel. The equations (14) and (15) can be used to write equation (13) in the form

$$z = \frac{dC_B}{d\tau} = k \frac{(\sigma - x)\, B_o}{\mu_T V} \cdot \left(\frac{1}{\beta} - x\right) \frac{0.21 \cdot L_o B_o}{V} \quad (16)$$

On the other hand, the speed of reaction can be determined from the rate of fuel consumption as :

$$-\frac{dC_B}{d\tau} = \frac{dx}{d\tau} \cdot \frac{B_o}{\mu_T V}$$

Since $\tau = \frac{\varphi}{6n}$, then $\frac{dx}{d\tau} = 6n \frac{dx}{d\varphi}$

and therefore,

$$-\frac{dC_B}{d\tau} = 6 \cdot n \frac{B_o}{\mu_T V} \cdot \frac{dx}{d\varphi} \quad .. \quad .. \quad (17)$$

By equating the expressions (16) and (17) we obtain

$$\frac{dx}{d\varphi} = k \cdot \frac{\sigma - x}{6n} \left(\frac{1}{\beta} - x\right) \frac{0.21 \cdot L_o B_o}{-V} \quad (18)$$

This differential equation permits the determination of the rate of fuel consumption $\frac{dx}{d\varphi}$ at any instant of the process, if the constant of reaction speed k and the amount σ and x, that is, the respective admitted and consumed fuel quantities are known. Vice versa, if the values for $\frac{dx}{d\varphi}$, σ, and x are determined by test, formula (18) can then be used to determine the momentary magnitude of the reaction speed constant k :

$$k = \frac{6n}{(\sigma - x)\left(\frac{1}{\beta} - x\right)} \cdot \frac{V}{0.21 \cdot L_o \cdot B_o} \cdot \frac{dx}{d\varphi} \quad .. \quad (19)$$

Formula (18) can also be written

$$\frac{dx}{(\sigma - x)\left(\frac{1}{\beta} - x\right)} = k \frac{0.21\, L_o\, B_o}{6\, n\, V} \cdot d\varphi \quad .. \quad (18a)$$

If a small angular difference $\varphi_2 - \varphi_1$ is considered, and if σ, K and V are assumed to possess the constant average values $\sigma_{1\text{-}2}$, $k_{1\text{-}2}$, and $V_{1\text{-}2}$ during this interval, then, according to Neumann, equation (18) can be integrated to yield

$$x = \frac{C.\sigma_{1\text{-}2} - \frac{1}{\beta} e^{-m_{1\text{-}2}\varphi}}{C - e^{-m_{1\text{-}2}\varphi}} \quad .. \quad .. \quad .. \quad (20)$$

where C is the integration constant determined by the initial conditions $x = x_1$ for $\varphi = \varphi_1$, and $x - O$ for $\varphi = \varphi_o$.

Then

$$m_{1\text{-}2} = \frac{0.21\, L_o\, B_o}{6\, n} \cdot \frac{k_{1\text{-}2}\left(\frac{1}{\beta} - \sigma_{1\text{-}2}\right)}{V_{1\text{-}2}} \quad .. \quad (21)$$

The amount of fuel x_2 consumed until the crankshaft turned to angle φ_2 is given by

$$x_2 = \frac{\sigma_{1\text{-}2} \dfrac{1/\beta - x_1}{\sigma_{1\text{-}2} - x_1} - \dfrac{1}{\beta} e^{-m_{1\text{-}2}(\varphi_2 - \varphi_1)}}{\dfrac{1/\beta - x_1}{\sigma_{1\text{-}2} - x_1} - e^{-m_{1\text{-}2}(\varphi_2 - \varphi_1)}} \quad .. \quad (22)$$

For the practical application of equation (22), it is necessary to know $\sigma = f(\varphi)$, $k = f_2(\varphi)$, $V = f_3(\varphi)$, and the time of ignition delay. The analytical expression for the admission of the fuel in a given injection system can be determined only by test; the ignition delay must also be found from a test. The variation of the cylinder $V = f_3(\varphi)$ is easily established by computation. With regard to the numerical determination of the momentary values of the reaction speed constant, it will be seen from equations (5) and (12b) that the functional relationship between the energy of activation Qa and φ must be known. Unfortunately this relationship has not been determined as yet, so that it remains necessary to resort to experimental data. Also, the factors influencing the length of the reaction and the characteristics of the latter as such are not yet fully explained. According to the investigations made by Neumann and by Inozemtsev, the variation of the reaction constant k with the crankshaft angle can be expressed by $k = a\, e^{b\varphi}$, where a and b are constants which can be determined from numerical values of k for commencement and termination of the reaction. The latter may be obtained with the use of the equations (5) and (12b). In this case the magnitude of the energy of activation at the extreme points of the combustion process remains unknown for the present. Also unknown is the magnitude of the total angle of combustion which introduces still another unknown factor into the computation.

According to the test results obtained by Neumann on a slow-speed diesel engine of 50 h.p. at 300 r.p.m. (which had a bore of 280 mm. and a stroke of 450 mm. and a compression ratio of 12), $\log k = 2 \cdot 854 + 0.0241\varphi$ and $k = .7^{13}\, e^{0.0555\varphi}$. From the diagrams obtained by Inozemtsev on a Jumo-4 aviation diesel, it is possible to derive the average value of $\log k \approx 3.7 + 0.034\varphi$ and $k \approx 5000 \cdot e^{0.0785\varphi}$

The very large differences in the expressions for the constant of reaction speed can be explained by the different temperatures and pressures prevailing in the individual cases. Thus, for instance, the compression ratio has a value of 17 in the case of the Jumo engine, which was also supercharged; while the engine investigated by Neumann had a compression ratio of 12 and was not supercharged. Similar uncertainties can be cleared up only with the help of accumulated experimental evidence and further refinement of the theory.

It remains to be mentioned that the entire heat of the fuel is not utilised in the combustion process; a portion of it is lost to the cylinder walls and spent on dissociation of the combustion products. Thus the heat usefully employed for increasing the internal energy of the gases and for producing external work is found as $x_1 = x - \Delta x_1 - \Delta x_2 = \psi x$ where Δx_1 is the amount of heat lost to the walls, Δx_2 is the amount of heat expended on the process of dissociation, and ψ is the coefficient of estimated heat utilisation at a given instant.

According to Inozemtsev, the coefficient ψ varies but little during the combustion process, decreasing gradually from 0.95 to 0.88, and amounting to $\psi = 0.9$ on the average. The coefficient ψ equals the coefficient of generated heat ξ only at the termination of the combustion process where $x = 1$.

According to the first law of thermodynamics, $dQ = Gc_v\, dT + Ap\, dV$ and $dQ = B_o\, H_u\, \psi\, dx$ where H_u is the lower calorific value of 1 kg. of fuel. Thus,

$$B_o\, H_u\, \psi\, dx = Gc_v\, dT + Ap\, dV \quad .. \quad (24)$$

As $dT = \frac{pdV + Vdp}{GR}$, equation (24) can also be written

$$B_o\, H_u\, \psi\, dx = \frac{A}{k - 1}(kp\, dV + V\, dp)$$

or

$$B_o H_u \psi \frac{dx}{d\varphi} = \frac{A}{k - 1}\left(kp \frac{dV}{d\varphi} + V \frac{dp}{d\varphi}\right)$$

where $k = \frac{c_p}{c_v}$

We must now consider the expression

$$\frac{dp}{d\varphi} = \frac{k-1}{AV} B_o H_u \psi \frac{dx}{d\varphi} - k \frac{P}{V} \frac{dV}{d\varphi} \quad .. \quad (25)$$

The cylinder volume is given by the relationship

$$V = V_c + \frac{V_h}{2}\left(1 - \cos\varphi + \frac{\lambda}{2}\sin^2\varphi\right)$$

where φ is the crankshaft angularity relative to the lower dead centre, V_c is the clearance volume and $\lambda = r/L$. The equation of the cylinder volume can also be written

$$V = \frac{V_h}{2}\left(\frac{\epsilon+1}{\epsilon-1} - \cos\varphi + \frac{\lambda}{2}\sin^2\varphi\right)$$

from whence it is found

$\frac{dV}{d\varphi} = \frac{V_h}{2}\left(\sin\varphi + \frac{\lambda}{2}\sin 2\varphi\right)$. Introducing these values for V and $dV/d\varphi$ into equation (25) and making $A/2 = 1/854$, we have

$$\frac{dp}{d\varphi} = \frac{854\,(k-1)\,\beta_o H_u \psi}{V_h\left(\frac{\epsilon+1}{\epsilon-1} - \cos\varphi + \frac{\lambda}{2}\sin^2\varphi\right)} \frac{dx}{d\varphi} - k \frac{p\left(\sin\varphi + \frac{\lambda}{2}\sin 2\varphi\right)}{\frac{\epsilon+1}{\epsilon-1} - \cos\varphi + \frac{\lambda}{2}\sin^2\varphi} \quad .. \quad (26)$$

This equation permits the computation of the rate of pressure increase at any instant of the combustion process, as all pertinent factors are known. Accurate results will be obtained if the computation is carried out for angular intervals of 2–3 degrees. By integrating the curve of the function $dp/d\varphi = f(\varphi)$ thus obtained, the relationship $p = f(\varphi)$ is arrived at, which represents the part of the indicator diagram covering the process of combustion.

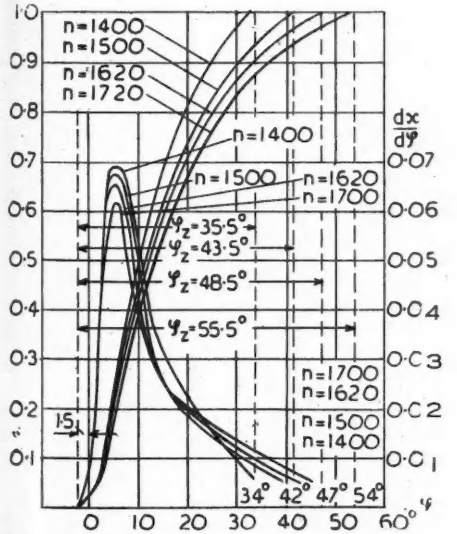

Fig. 1. **Curves for $x = f(\varphi)$ and $dx/d\varphi$ attained with Jumo-4 engine.**

With the joint use of test results and computed data, Neumann has succeeded in rendering graphs which include all the factors that are required for the kinetic analysis of the combustion process, and he has shown that the computed relationship $x = f(\varphi)$ agrees very well with actual diagram data. Good agreement between computed and experimental data was also obtained by Inozemtsev in his investigation of the Jumo-4 engine, the experimental results of which are charted in Fig. 1. In Fig. 2 these data are compared

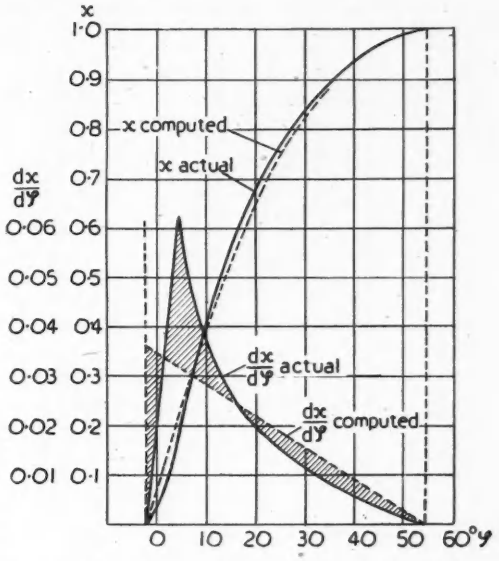

Fig. 2. **Comparison of the test results of Fig. 1 with Neumann's formulas.**

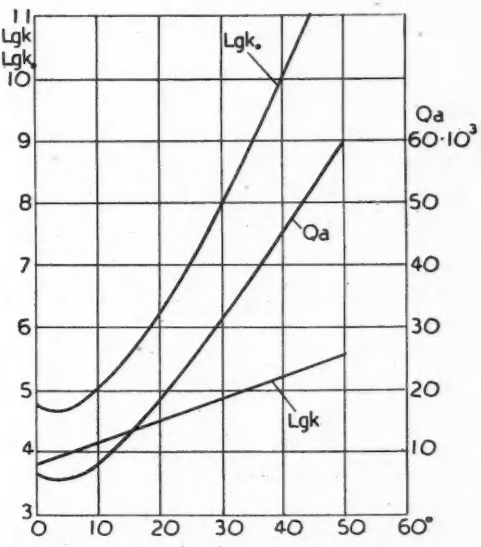

Fig. 3. **Factors k_1 k_o and Q_a as function of the crank angle.**

with the theoretical curves derived from Neumann's equations. The variations of log k, log k_o, and of Q_a with the crank angle are charted in Fig. 3, this chart being derived from a Jumo 4 running at 1700 r.p.m. Average values of these factors for a speed range of 1400-1700 r.p.m. are given in Fig. 4 in which the abscissa is made to represent the relative angularity φ/φ_z. From Fig. 3, and also from Neumann's graphs, the initial energy of activation Q_a is found to amount to 5,000 – 6,000 kal per kg-mol at the commencement of the reaction, while it rises to 50,000–55,000 kal per kg-mol towards the termination of the reaction. The diminution in the energy of activation which occurs at the commencement of the reaction is explained by Neumann as being due to chemical processes which take place during the ignition delay. Both the constant k of the actual speed of reaction (based upon the number of effective activating collisions) and the constant k_o derived from the kinetic theory (based on the total number of collisions) increase during the combustion period. Thus towards the end of the combustion period, the constant k_o attains an upper limit value of 10^{11}–10^{12} which corresponds to a purely gaseous reaction. For this reason, the final phase of the combustion process may be considered to represent a homogeneous reaction. Neumann has shown that the temperature coefficient of the constant of the reaction speed has an average value of $(k_T + 10°)/k_T = 1.01 - 1.07$. This compares with a value of 2 – 3 given by Van't Hoff for the case of a completely homogeneous reaction.

This discrepancy can be explained by the fact that in the diesel engine the reaction is of the heterogeneous type for a considerable length of time—a fact proven by spectroscopic investigation.

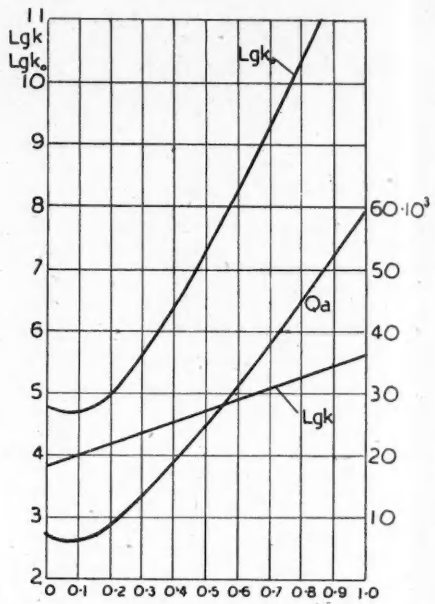

Fig. 4. **Factors k_1 k_o and Q_a as function of the relative crank angle φ/φ_z.**

THE INFLUENCE ON TENSILE STRENGTH OF THE INCLINATION OF WELD-SEAMS TO THE DIRECTION OF LOADING.

By H. ZSCHOKKE and R. MONTANDON, Brown-Boveri & Co., Baden. (From *Schweizer Archiv*, Vol. 10, No. 5, 1944, pp. 129-137).

INTRODUCTION.

IN calculating the strength of welded joints, it is customary to assume that the allowable load perpendicular to the seam is lower than that in the direction of the seam. If the seam, originally perpendicular to the tensile load, is gradually inclined towards the direction of load, the stress component perpendicular to the seam decreases until it becomes zero. Thus, by inclining the weld seam, the load carrying capacity of the joined sheets increases, or what amounts to the same, thinner sheets can be employed. Of particular interest in this connection, is the seam efficiency which is the ratio of seam strength to the strength of the materials to be joined. Obviously, the possible gain by increasing the inclination is the greater, the lower the seam efficiency. For a seam efficiency equal to one, the inclination of the seam is of no advantage.

The purpose of the present investigation was to find experimentally for various seam efficiencies, that angle of inclination of the seam which results in the greatest static tensile strength.

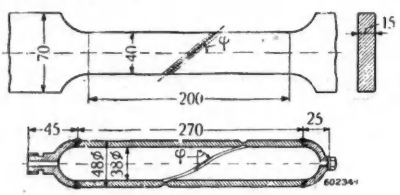

Fig. 1. **Test samples.**
Top : flat bar. Bottom : pressure vessel.

TYPE AND RANGE OF TESTS.

Tests have been made with flat bars under tension, and with small pressure vessels subjected to internal pressure. On these samples, according to Fig. 1, the angle φ was varied systematically, which offered no difficulty. However, the other variable, namely the seam efficiency, could not be varied without employing a trick, as it is not possible to produce weld seams of a predetermined and constant degree of deficiency. The trick consists of substituting for the weld seam a suitable weakening of the material, e.g., a groove on both sides. Thereby the modulus of elasticity is maintained, yet a notch effect is produced which is qualitatively and quantitatively equivalent to a weld deficiency. This had to be proved by preliminary tests.

The following tests were made whereby the angle φ between the seam and the direction of tensile load was varied from 0 to 90 deg., and the seam efficiency was in the range from 1 to 0.4 :

(A) Comparison between weld defects and grooves ;
(B) Flat bars unwelded and welded, weld seam unmodified and seam machined ;
(C) Flat bars, and pressure vessels unmodified and with 20 per cent and 60 per cent groove depths.

The grooves and their dimensions are shown in Fig. 2. The material for tensile tests was M1 sheet used for boilers, of 40 kg./mm.² ultimate tensile strength, and for the pressure vessels, tubes of St. 35.29, the ultimate tensile strength of which after annealing was 34 kg./mm.² Throughout, stresses have been related to full cross sections. This applies to both flat bars and pressure vessels ; for the latter, stresses refer to the inner surface of the vessel.

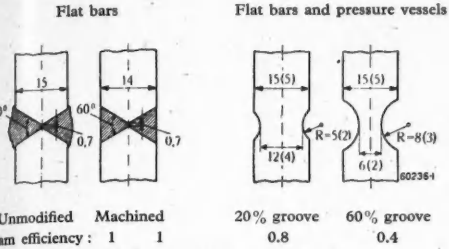

Fig. 2. **Shape of weld bead and groove shape.**

(A) Preliminary tests. Comparison of weld defects with grooves.

The authors undertook extensive investigations (omitted here) which proved that weld defects can be compared with notch effects. Static loading has been considered only, and for the present purpose it has been shown that a weld defect of 20 per cent of the wall thickness has little effect on the static load carrying capacity, whereas the elastic properties are changed by a mere 10 per cent. For subsequent tests the relationship has been established between the grooves used and the welds they are to represent, so that the results with inclined grooves can be translated into corresponding weld results. The elasticity of the weld and of the joined material is about equal up to the yield point. Apprehensions as to a lower ductility of the weld seam appear to be unjustified, as due to the high safety factors employed in boiler design, the plastic range concerning this is never reached.

(B) Tests on welded flat bars.

Two series of tensile tests have been made with unmodified seams and with machined ones. The seam efficiencies were equal to one. Fracture then occurs at some distance from the seam owing to restricted lateral construction of the weld. The load carrying capacity is equal to or higher than that of an unwelded specimen (Table 1). Figs. 3 and 4 show the fractured specimens, and it can be seen that for seam efficiencies of one, the inclination of seam is immaterial. It is to be emphasised that the welds have not been heat-treated.

TABLE 1. TENSILE STRENGTH OF FLAT BARS FOR VARIOUS ANGLES φ.

Angle φ deg.	Tensile strength kg/mm.² for				
	Bar unwelded	Bar welded unmodified	Bar welded weld machined	Bar with 20 per cent grooves	Bar with 60 per cent grooves
0	39.6	—	—	—	—
30	39.6	39.9	40.9	38.8	23.6
45	39.6	39.4	39.4	39.5	19.3
60	39.6	39.6	39.6	37.8	19.2
90	39.6	41.2	39.9	38.5	21.6

(C) Tests on flat bars and pressure vessels, with 20 per cent and 60 per cent grooves.

Samples with 20 per cent grooves (seam efficiency = 0.8) show that there is very little reduction in the load carrying capacity of bars (Table 1) and pressure vessels (Table 2), and, accordingly, only a slight dependence on the angle φ. The test results are shown diagrammatically in Fig. 5. Figs. 6 and 7 show the fractured specimens. With increasing angle φ, the onset of fracture is first in the direction perpendicular to the direction of principal tension, then, partly by slipping, in the plane of the groove. Actually, fracture in the plane of the groove takes place at large angles. With samples of 60 per cent grooves (seam efficiency 0.4) the load carrying capacity is essentially reduced, and is greatly dependent on the angle φ (Tables 1 and 2 and Fig. 5). The fractured specimens are shown in Figs. 8 and 9. Similarly, as in the 20 per cent grooves, there is a shift in the position of the fracture with increasing angle φ. In the transition region between oblique and longitudinal fracture, a repeated change between the two types often takes place (Fig. 10).

TABLE 2. FAILURE STRESS OF TEST VESSELS UNDER INTERNAL PRESSURE FOR VARIOUS ANGLES φ.

Angle φ deg.	Failure stress kg./mm.² for					
	Vessel without grooves		Vessel with 20 p.c. grooves		Vessel with 60 p.c. grooves	
	inner surface	outer surface	inner surface	outer surface	inner surface	outer surface
0	33.7	25.9	33.5	25.8	31.9	24.5
30	33.7	25.9	33.6	25.8	24.2	18.6
45	33.7	25.9	33.7	25.9	21.6	16.6
60	33.7	25.9	33.2	25.5	19.1	14.7
90	33.7	25.9	33.0	25.4	19.7	15.2

Failing stresses determined according to formula :

$$\sigma_t = \frac{p_i \cdot r_i^2}{r_o^2 - r_i^2}\left(1 + \frac{r_o^2}{r_i^2}\right) \quad \text{inner surface}$$

$$\sigma_t = \frac{2p_i \cdot r_i^2}{r_o^2 - r_i^2} \quad \text{outer surface}$$

where σ_t = failing stress, p_i = internal pressure, r_o = outer radius, r_i = inner radius

The fact that below a certain angle φ there is no notch effect could also be proved, in so far as by slipping in the plane of groove, the cylinder is opened up helically (Fig. 12). Illustrations are shown on pages 50 and 51.

CONCLUSIONS.

The above tests have shown that for a seam efficiency of 0.8, the maximum reduction in the load carrying capacity of flat bars is 4.5 per cent and of pressure vessels 2.1 per cent. For a seam efficiency of 0.4 the load carried is 54 per cent for flat bars, and 58 per cent for pressure vessels of the load sustained by unwelded samples. Thus, in boiler design, there is no reason to employ inclined (helical) weld seams as with the realized seam efficiencies of 1 to 0.7 the possible gain by inclined welds is by far outweighed by economical disadvantages (longer weld seams, losses by cutting the sheet metal).

Inclined weld seams seem to be of advantage only in special cases, such as, with high strength material of bad weldability (low seam efficiency). On the whole, in normal pressure vessel design and with pure static loading, an apprehensive over-estimation of weld defects is out of place.

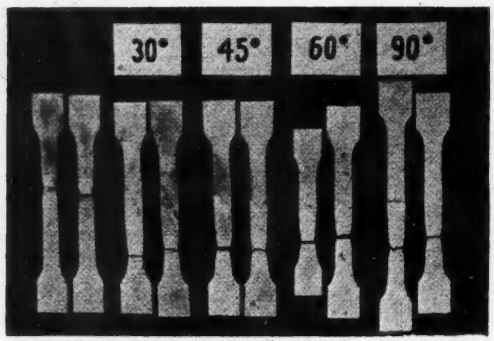

Fig. 3. **Flat bars with unmodified weld seams after failure.**

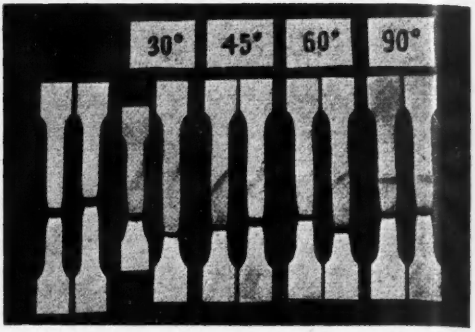

Fig. 4. **Flat bars with machined weld seams after failure.**

TENSILE TEST ON FLAT BARS
Stresses related to unweakened cross section.

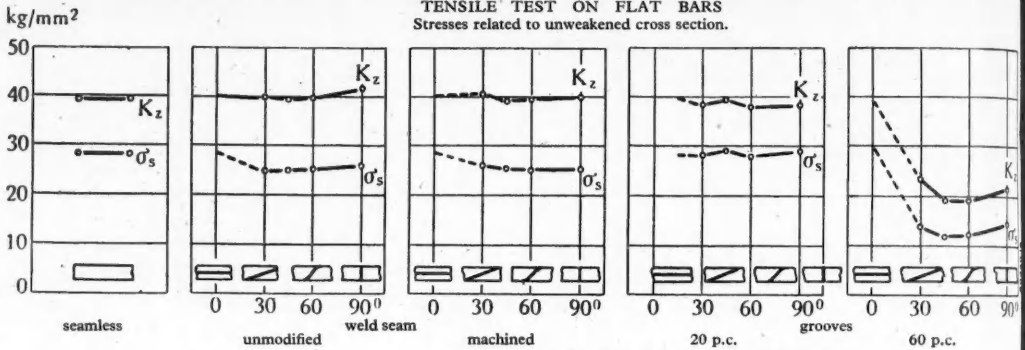

PRESSURE TEST ON VESSELS
Stresses at inner surface and referred to full wall thickness.

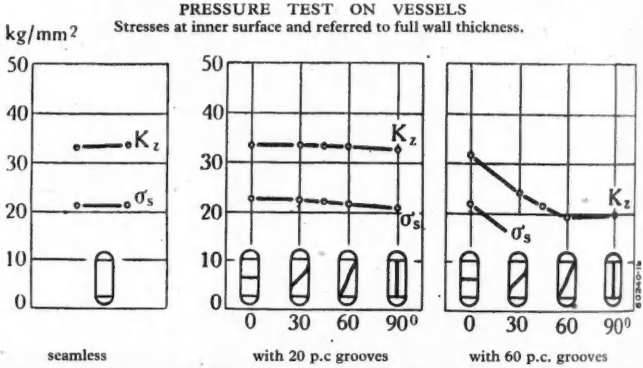

Fig. 5. **Strength of flat bars and pressure vessels for various seam and groove angles.**

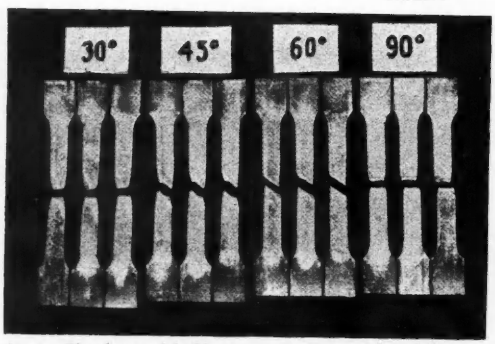

Fig. 6. **Flat bars with 20 per cent grooves after failure.**

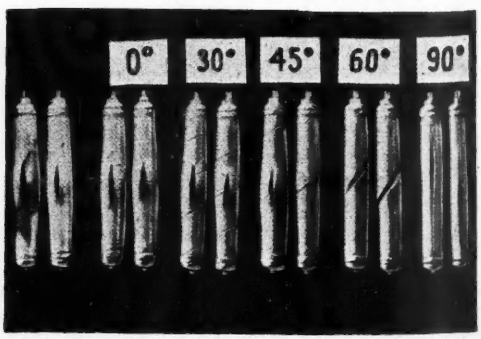

Fig. 7. **Pressure vessels with 20 per cent grooves after failure.**

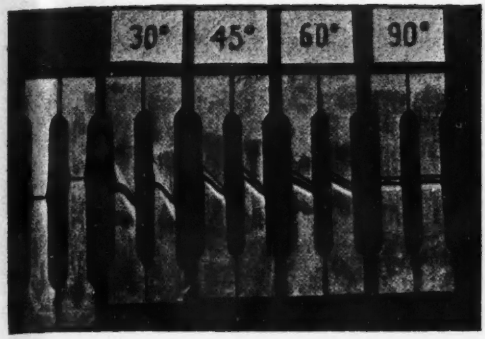

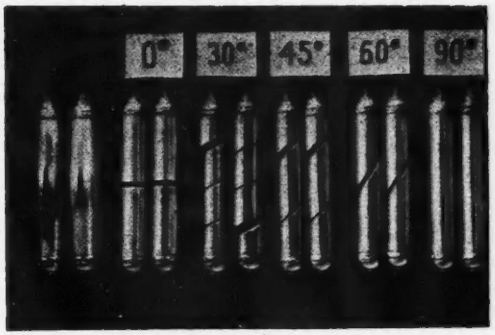

Figs. 8 & 9. **Flat bars and pressure vessels with 60 per cent grooves after failure.**

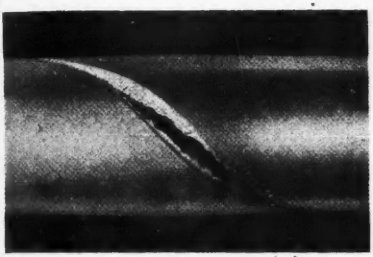

Fig. 10. **Pressure vessel with 20 per cent groove, φ = 60 deg. after failure.**

Fig. 11. **Pressure vessel with 20 per cent groove, φ = 60 deg after failure.**

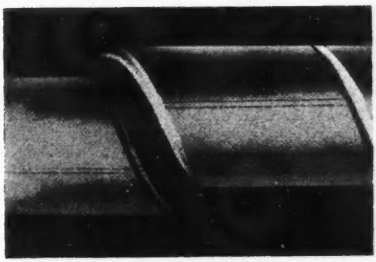

Fig. 12. **Pressure vessel with 60 per cent groove, φ = 30 deg. after failure.**

THE EQUILIBRIUM CONDITION OF MANOMETERS OF THE RING BALANCE TYPE

By Dr. H. WILDE. (From *VDI Zeitschrift*, Vol. 83, March, 1944).

Two different explanations of the working principle of the ring balance type manometer are given in technical literature. According to the first of these explanations, it is the torque exerted upon the division wall which causes rotation of the balance; while the other explanation states that the rotation is due to the turning moment which is caused by the displacement of the centre of gravity of the manometric liquid contained in the ring. According to the explanation chosen, different and apparently contradictory analytical solutions of the working characteristics of the ring balance have been established. In view of this unsatisfactory state of affairs, both concepts of the operating principle will be investigated, and it will be shown how the equilibrium conditions can be conveniently expressed analytically.

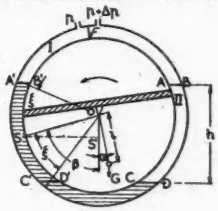

Fig. 1. **Ring balance.**

Referring to Fig. 1, it is assumed that the ring balance is centrally supported, that its sectional area is constant throughout, and that the disposition of its mercury content corresponds to a pressure difference Δp. The pressure prevailing in air space I may be denoted by p, and that in space II by $p + \Delta p$. The corresponding pressure distribution in the mercury will then be that shown in Figs. 2 and 3. To this must be added the gravitational pressure effect caused by the weight of the mercury which causes the pressure to rise in linear proportion with the height of the mercury column. The pressure distribution is uniform throughout, except the pressure differential across the compartment wall F.

Figs. 2, 3. **Pressure distribution in ring balance supplied with (Fig. 2) air or (Fig. 3) water.**

As the pressure of a gas or a liquid can only act in perpendicular direct upon a containing wall, the only pressures exerted will be the pressures p and $p + \Delta p$ acting upon the respective sides of the division wall. The difference in liquid levels, that is the manometric height h, causes the gas to transmit a pressure upon the division wall, the resultant turning moment being given by $\Delta p.q.R = h(\gamma_1-\gamma_2)q.R$ where q is the surface area of the division wall, R is the distance of the latter from the fulcrum of the balance, γ_1 is the specific gravity of the manometric liquid of the balance, and γ_2 is that of the medium (gas or liquid), the pressures of which are applied to the balance. Also, $\Delta p = h(\gamma_1-\gamma_2)$ is the pressure differential. No turning moment is exerted by the atmospheric air surrounding the balance.

The turning moment resulting from the application of the pressure differential causes the balance to rotate by the angle α until equilibrium is established with the oppositely directed turning moment of the deadweight of the balance. For an angle α with the zero position, the turning moment caused by the deadweight is given by $G \cdot l \cdot \sin \alpha$, where l is the leverage of the deadweight. The equilibrium condition of the ring balance is, therefore, given by

$$G \cdot l \cdot \sin\alpha = h\ (\gamma_1-\gamma_2) \cdot q \cdot R$$

If the balance consists of a semi-circle as indicated in Fig. 4, there will be two confining end walls instead of one division wall F, but this does not affect the equilibrium condition as such.

The same equilibrium equation can also be obtained by deriving the turning moment from the displacement of the weight of the manometric fluid. In this case the liquid may be assumed to be rigidly connected with the balance element. By multiplying the respective weights of the fluids contained in the spaces ABCD and $A^1B^1C^1D^1$ with the lengths of the respective levers, the turning moment is found as $h \cdot q\ (\gamma_1-\gamma_2)R$, where R is the mean radius of the balance. Referring to Fig. 1, this result is found as follows: With point S representing the centre of gravity of the fluid column $A^1B^1C^1D^1$, it is

$$\overline{OS} = \frac{\int_0^{\xi} R \cos x \cdot dx}{\int_0^{\xi} dx} = R\frac{\sin \xi}{\xi}$$

The effective length of the lever is then found as

$$\overline{SS} = \frac{R \cdot \sin \xi}{\xi} \sin \beta$$

while the weight of the fluid is $G = 2.q \cdot \gamma \cdot R \cdot \xi$. But it is also $h = R\ [\cos(\beta - \xi) - \cos(\beta + \xi)] = 2 \cdot R \cdot \sin\beta \cdot \sin\xi$

The turning moment therefore becomes

$$G \cdot \overline{SS} = 2{:}q \cdot \gamma \cdot R \cdot \xi \frac{R \cdot \sin \xi}{\xi} \sin \beta = h \cdot q \cdot \gamma \cdot R$$

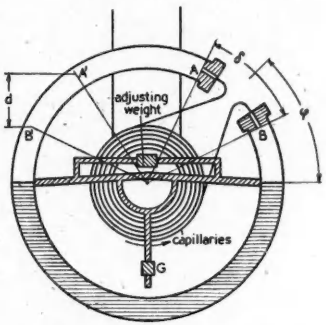

Fig. 4. **I.G. High pressure ring balance in zero position.**

In most cases the actual design of the balance, such as that shown in Fig. 4, does not include a division wall. This concept should not, therefore, be used, as it is quite misleading. Considering, for instance, the case in which the balance is used to measure the differential pressure across an orifice, the orifice itself will represent the division wall with regard to the pressure differential.

Different considerations apply to pressure balances which are not centrally supported and to such which have cross section of unequal area, as they are used in special cases. In balances of these types the forces responsible for turning moments are not limited to confining end walls. Referring to Fig. 5, which shows such a balance, the centre of gravity of the balance element is seen to coincide with the point of rotation,

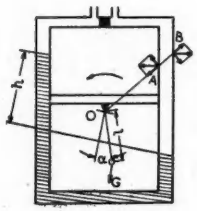

Fig. 5. **U-type ring balance.**

the counter torque being solely supplied by the weight G. Here the perpendicular pressure forces, as shown for instance in points A and B include an angle with the line OA, and they can, therefore, be replaced by component forces, of which one acts in the direction OA and the other in a direction perpendicular with OA. Of these the component forces in the direction OA will obviously be unable to exert a turning moment; and a turning moment will be caused only by the other perpendicular components.

BRAKING AIRSCREW AND HIGH-SPEED FLIGHT

By Dipl. Ing. A. Von der Mühll, Airscrew Division of the Escher Wyss Co., Zurich. (From *Flugwehr und-Technik*, No. 6, June, 1944, pp. 173-177).

This article is the last in a series reviewing the improvements in aircraft design due to the progress made by the Escher Wyss braking airscrew in shortening the landing run.

The first article [1] * on flight tests have shown that not only was the landing run reduced, but also the safety in landing was increased, even at higher landing speeds, and thus, higher wing loading can be employed [2]. The difficulties of landing highly loaded aircraft being alleviated, it seemed that the difficulties shifted to the take-off. It was, therefore, of interest to prove that the variable pitch airscrew gives the answer to the take-off problem too. To this end a new method has been developed to enable the static thrust of a variable pitch airscrew to be accurately predicted. This method indicates the principles on which the aero engine should be designed to give considerably increased static thrust at constant power [3] and which increase in static thrust secures the take-off of highly loaded aircraft [4]. The present article deals with the determination of the possible speed increase with an increase in wing loading.

Airplane Characteristics.

The most important dimension of an aircraft, namely, its wing area, is not determined by requirements of flight, but by those of take-off and landing. Nature knows no such barriers where aerodynamic merits are concerned. For instance, some birds of great wing span like the albatros and swallow are unable to take-off from flat ground. They start from elevated points. Disregarding special designs, airplanes will generally start from earth level. Their main task is the transport of passengers and high-class goods to distances at high speed. In the conventional airplane an increase in speed beyond certain limits had, until recently, two principal limitations:

1. The power required for producing lift and to overcome drag cannot be arbitrarily increased because of the increasing fuel consumption which sets a limit to power increase by reducing the range.
2. Drag cannot arbitrarily be reduced as the wing itself contributes extensively to the total drag. As aircraft are earthbound no great changes are possible in reducing the wing dimensions.

Investigating the possibilities to increase speed, the following conclusions are reached. In a speed range of 200 to 850 km/hr., airscrew efficiencies of over 80 per cent can be obtained. The thermal efficiency of the conventional aero engine is, according to fuel consumption, (175 to 250 gramms/h.p. hr.), 25 or 35 per cent. Of the energy of the fuel, the engine thus transforms 20 to 32 per cent into thrust. The exhaust efflux propulsion is not included in this figure, but at high speed it brings an increase of the above percentage which should not be neglected.

The restrictions listed under 1 could be alleviated only if it were possible to increase the thrust without increasing the fuel consumption. Surprisingly, the second restriction can be narrowed down by using the airscrew as a brake in landing [1, 2] and by augmenting the static thrust [3, 4]. These factors indirectly contribute to a reduction in wing drag, inasmuch as the wing can be designed for requirements of flight and disregarding the fact that airplanes are "earthbound." Present-day wing loadings of 150 to 200 kg/sq. m. are still below the optimum values in high speed flight, and were obtained by considering the requirements of landing. By the use of braking airscrews the wing loading can be increased to its optimum value. Simple formulae will show these matters quantitatively, and are, therefore, included here.

Equations of Flight Mechanics.

The few equations required here can be derived from the condition of equilibrium (Fig. 1). The horizontal speed is then,

$$V = \sqrt[2]{\frac{G/F}{\rho/2.\ Ca}} \quad .. \quad .. \quad .. \quad (1)$$

where

G	=	Weight of aircraft	(kg)
A	=	Lift	(kg)
Ca	=	Lift coefficient	(—)
V	=	Speed	(m/sec)
F	=	Wing area	(m^2)
ρ	=	Density	(kg. sec^2/m^4)

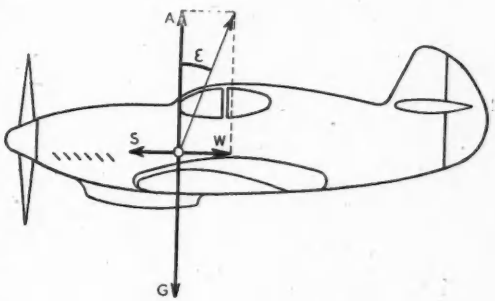

Fig. 1

The landing speed can be taken as the smallest horizontal speed (i.e., with landing flaps down) and equation (1) becomes

$$V_L = \sqrt[2]{\frac{G/F}{\rho_L/2.\ Ca_L}} \quad .. \quad .. \quad .. \quad (2)$$

where index L denotes landing.

*Numerals in brackets [ ] indicate literature references at the end of the article.

The horizontal speed can also be expressed as

$$V = \sqrt[3]{\frac{N.\eta}{\rho/2\ F.C_w}} \quad .. \quad .. \quad (3)$$

where the additional symbols are

N = Effective engine power (mkg./sec.)
η = Airscrew efficiency (—)
C_w = Drag coefficient (—)

The maximum horizontal speed V_h is obtained if the full throttle power, $N.\eta_h$ is substituted into eq. (3) at ρ_h, that is, the density at maximum altitude for which this power is available. The corresponding drag coefficient is C_{wh}.

To determine the aerodynamic coefficients Ca_h and C_{wh} we have the equation

$$\frac{N\eta}{G} = \sqrt[2]{\frac{G/F.}{\rho/2} \frac{C_w^2}{Ca^2}} \quad .. \quad .. \quad .. \quad (4)$$

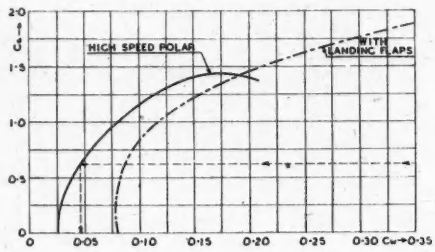

Fig. 2

For a given aircraft, the wing area, the weight of the aircraft and its polare are given (Fig. 2). The engine power and airscrew efficiency are known by their characteristics (for high speed flight $\eta_h = 0.8$ is first assumed). Thus, eq. (4) can be solved for Ca_h^3/C_{wh}^2, and from an auxiliary diagram (Fig. 3) plotted from the polare, Ca_h can be read off. For this value of Ca_h, Cw_h is found from Fig. 2. With Cw_h thus obtained, the maximum horizontal speed according to eq. (3) can be calculated

$$V_h = \sqrt[3]{\frac{N.\eta_h}{\rho_h/2.\ F.\ Cw_h}} \quad .. \quad .. \quad .. \quad (3a)$$

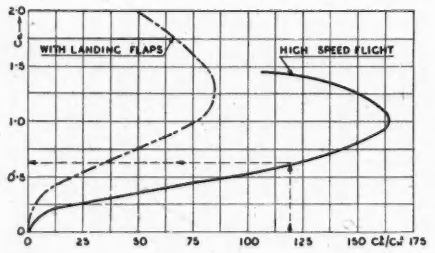

Fig. 3

The speed range

Based on considerations given previously one might think that by introducing the braking airscrew, the maximum speed and landing speed increase in the same ratio. That this is not quite the case can be seen by eqs. (3a) and (2). Then, the speed range Δ can be written

$$\Delta = \frac{V_h}{V_L} = \frac{\sqrt[3]{\frac{N/F.\ \eta_h}{\rho_h/2.\ Cw_h}}}{\sqrt[2]{\frac{G/F}{\rho_L/2.\ Ca_L}}} \quad .. \quad .. \quad .. \quad (5)$$

This equation can be transformed to

$$\Delta = \sqrt[6]{F} \frac{\sqrt[3]{N.\ \eta_h} \quad \sqrt[2]{\rho_L/2} \quad \sqrt[2]{Ca_L}}{\sqrt[2]{G} \quad \sqrt[3]{\rho_h/2} \quad \sqrt[3]{Cw_h}} \quad .. \quad (6)$$

Equation (6) shows that the speed range does not only depend upon the aerodynamic figure of merit (Ca^3_L/Cw^2_h), the densities near ground and at the rated altitude, but also upon the available power ($N.\eta_h$), the weight (G) and the wing area (F). As shown by eq. (5) an increase of the speed range is obtained with greater advantage by reducing the landing speed rather than by increasing the maximum speed. This being so because the former expression is under the square root, whilst the latter is under the cube root.

In flying contests the speed range has repeatedly been used as a performance criterion. Crash landings at low speed are, as experience has shown, so much less dangerous and, therefore, the application of the conception of speed range is a correct one. As an absolute measure for comparing two airplanes, the speed range has meaning only if the two planes are either of equal maximum speed or of equal landing speed. Typical examples of such contests were the Guggenheim contest (1928) and the flight around Europe (1934).

In other contests such as the Coupe Deutsch (1934) the aim of the race was directed towards the development of high speed aircraft. In these races, and later in civil aviation, the endeavour for increase in maximum speed, though reducing the speed range, has proved compatible with requirements of safety.

(To be continued).

[1] Von der MÜHLL, A.: The Airscrew as a Landing Brake, *Flugwehr und Technik*, Vol. 5, No. 2 (1943), pp. 51-54. Also: "*The Engineers' Digest*," Vol. 4, No. 8 (1943), pp. 231-232.

[2] Von der MÜHLL, A.: The Effectiveness of the Airscrew as a Landing Brake, *Flugwehr und Technik*, Vol. 5, No. 8 (1943), pp. 211-217. Also: "*The Engineers' Digest*," Vol. 5, No. 4 (1944), pp. 115-117.

[3] ROTH, Franz: A Method of Estimating the Static Thrust of Airscrews, *Flugwehr und Technik*, Vol. 5, No. 10 (1943), p. 265.

[4] ROTH, Franz: The Influence of Airscrew Thrust on Take-off Distance, *Flugwehr und Technik*, Vol. 6, Nos. 1 & 2 (1944), pp. 23-28 and 52-54. Also: "*The Engineers' Digest*," Vol. 5, No. 10 (1944), pp. 299-302.

[5] BELART, H.: High Wing Loading, *Aircraft Engineering*, June, 1938.

[6] HAUSAMMANN, W.: Drag Problems in Present Day Aircraft Design, *Flugwehr und Technik*, Vol. 4, No. 7 (1942), pp. 179. Also: "*The Engineers' Digest*," Vol. 3, No. 12 (1942), pp. 424-427.